

AFML-TR-79-4122

2
R

LEVEL H

AD A080607

LIQUID AND SOLID PARTICLE IMPACT EROSION

George F. Schmitt, Jr.

Coatings and Thermal Protection Materials Branch
Nonmetallic Materials Division

November 1979

TECHNICAL REPORT AFML-TR-79-4122

Final Report for Period March 1979 - June 1979

DDC FILE COPY

Approved for public release; distribution unlimited.

AIR FORCE MATERIALS LABORATORY
AIR FORCE WRIGHT AERONAUTICAL LABORATORIES
AIR FORCE SYSTEMS COMMAND
WRIGHT-PATTERSON AIR FORCE BASE, OHIO 45433

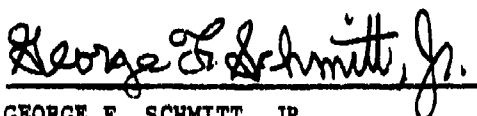
D'D'C
RECEIVED
FEB 14 1980
RECEIVED
A

80 2 11 023

NOTICE


When Government drawings, specifications, or other data are used for any purpose other than in connection with a definitely related Government procurement operation, the United States Government thereby incurs no responsibility nor any obligation whatsoever, and the fact that the government may have formulated, furnished, or in any way supplied the said drawings, specifications, or other data, is not to be regarded by implication or otherwise as in any manner licensing the holder or any other person or corporation, or conveying any rights or permission to manufacture, use, or sell any patented invention that may in any way be related thereto.

This technical report has been reviewed and is approved for publication.



GEORGE F. SCHMITT, JR.
Project Engineer

FOR THE COMMANDER:



J. M. KELBLE, Chief
Nonmetallic Materials Division
Air Force Materials Laboratory

"If your address has changed, if you wish to be removed from our mailing list, or if the addressee is no longer employed by your organization please notify AEML/MBE, W-P AFB, OH 45433 to help us maintain a current mailing list".

Copies of this report should not be returned unless return is required by security considerations, contractual obligations, or notice on a specific document.

AFML-TR-79-4122

FOREWORD

This report was prepared by George F. Schmitt, Jr. of the Coatings and Thermal Protection Materials Branch, Nonmetallic Materials Division, Air Force Materials Laboratory (MBE), Wright-Patterson Air Force Base, Ohio. The work was initiated under Project No. 2422, "Protective Coatings and Materials," Task No. 242201, "Coatings for Aircraft and Spacecraft." The report covers research conducted during the period March 1979 to June 1979. The report was submitted in July 1979.

This report was commissioned by the ASME Wear Control Handbook, a centennial project of the American Society of Mechanical Engineers, New York, N.Y. and is contributed by the author and the Air Force to that publication.

Accession No.	
No. of pages	2
Date	
Author	
Subject	
By	
Date of report	
Date of publication	
Availability	
1st	

TABLE OF CONTENTS

SECTION		PAGE
I	GENERAL DESCRIPTION OF EROSION PHENOMENA	1
II	MECHANISMS OF EROSION DAMAGE	3
	1. Liquid Impact	3
	2. Modes of Liquid Impact Damage	4
	3. Solid Impact on Ductile Metals	8
	4. Solid Impact on Brittle Metals	11
III	EROSION PREDICTION TECHNIQUES	15
	1. Thiruvengadam's Theory of Liquid Impact Erosion	15
	2. Springer's Theory of Liquid Impact Erosion	18
	3. Brittle Material - Liquid Impact Theories	20
	4. Hertzian Impact Theories	21
	5. Brittle Material Models	23
	6. Empirical Models	24
IV	EROSION DATA SOURCES	26
	1. Liquid Impact	26
	2. Solid Impact	27
V	MATERIALS PROPERTIES EFFECTS	29
	1. Metals	29
	2. Polymers	30
	3. Ceramics	31
VI	MATERIALS TO RESIST EROSION	33
	1. Metals	33
	2. Ceramics	34
	3. Elastomers	36
	4. Plastics	37
VII	DESIGN TECHNIQUES TO AVOID EROSION	38
	1. Reduction in Velocity	38
	2. Reduction in Impact Angle	38
	3. Reduction in Droplet Size or Particle Diameter	39
	4. Particle Concentration Reduction	39

TABLE OF CONTENTS (Cont)

SECTION	PAGE
5. Leading Edge Radius Effects	40
6. Flush Mounting/Gradual Bends	40
7. Geometry and Scale-up	41
VIII CONCLUSIONS	43
REFERENCES	44
BIBLIOGRAPHY	52

LIST OF ILLUSTRATIONS

FIGURE		PAGE
1	Damage Modes Due to Liquid Drop Impingement	54
2	Erosion Rate/Cumulative Erosion	55
3	Dependence of Erosion Rate on Attack Angle is Shown Schematically for Ductile and Brittle Materials	56
4	Impact of Rectangular Plate Showing Definitions of Impact Angle and Rake Angle	56
5	Sections Through Impact Craters Showing Typical Shapes	57
6	Thiruvengadam's Erosion Strength Estimator	57
7a	Schematic of the Experimental Results	58
7b	The Solution Model	58
8	Incubation Period Versus S/P	59
9	Comparison of Springer Model with Experimental Results	60
10	Pressure Distribution Under Impacting Water Drop	61
11	Comparison of Rain Erosion Behavior of the Different Material Classes	62
12	Rain Erosion of Some Glasses, Ceramics, and a Special Sapphire	62
13	Relative Erosion Performance of Commercially Available Metals	63
14	Ceramics (90-Deg Impingement)	64
15	Kennametal Cemented Carbides (90-Deg Impingement)	64
16	AFML Rotating Arm Apparatus	65

LIST OF TABLES

TABLE		PAGE
1	Impact Conditions for Water Drops	66
2	Description of Data and Symbols Used in Figures 8 And 9	67
3	Rain Erosion Equation Constants, Nose Tip Materials	70
4	Room Temperature Erosion Test Results	71
5	700 Degrees Centigrade Erosion Test Results	72
6	Room Temperature Erosion Test Results on Coated Materials	73
7	700 Degrees Centigrade Erosion Test Results on Coated Materials	73
8	Abbreviations Used in Tables 4 and 7	74

SECTION I

GENERAL DESCRIPTION OF EROSION PHENOMENA

Erosion of materials and components caused by the impact of liquid drops or solid particles can be a life-limiting phenomenon for the operation of systems in erosive environments.

Rain erosion or material damage due to flight through natural rainstorms has been a concern for aircraft and missiles since World War II. The impact of liquid drops which are condensed steam entrained in the airflow has been a major concern in the operation of large hydroelectric plant steam turbines for many years. Other systems in which liquid droplets of substantial size may impact material surfaces causing damage are also subject to erosive attack. An example would be a fuel injection device.

Solid particle impact erosion has been receiving increasing attention in recent years because of the research and development of coal conversion plants with their need for movement and flow of solid particles into various equipment in these plants. The impact of these particles on moving blades, valve constrictions, pipe joints and bends, and other surfaces has resulted in severe erosion. Solid particle erosion has been a concern for aerospace systems for many years including sand erosion on leading edges of helicopter blades, ingestion and erosion of leading and trailing edges of jet engine blades and vanes, and solid particle impacts on glass domes of captively carried, optically guided missiles or laminated plastic transparent windshields and canopies.

Coupled effects are a significant factor in the erosion of materials. Although they will not be treated in this section, they should be mentioned. An example is the combined corrosion/impact erosion experienced in coal conversion where most systems operate at elevated temperatures in environments which are quite corrosive and erosive. The sulfidation/oxidation/material removal due to impact mechanisms is extremely complex and not well understood.

Another example of coupled effects is the combined ablation-erosion for reentry vehicle nosetips and heat shields of high velocity missiles as they reenter the atmosphere and pass through high cirrus ice clouds or precipitating snow or rain. The erosion impact material removal and the ablative heat transfer/vaporization/thermomechanical removal occur essentially simultaneously and each influences the other by its effects on the material involved.

Beneficial uses of erosive processes are few but significant. Most people are aware of the use of sand blasting for cleaning purposes. However, the extent to which liquid jet cutting (an impact process using jets of liquid rather than discrete drops) has been adopted for mining, tunneling, cutting rock, cutting lumber, and advanced graphite-epoxy composite materials is not generally known. The use of liquid jets for digging pole holes or trenching for power utilities has been explored and found to be feasible and potentially cost effective.

This section will deal with the detrimental effects of liquid and solid particle impact erosion and ways of combatting this phenomenon.

SECTION II

MECHANISMS OF EROSION DAMAGE

The response of engineering materials to the impingement of liquid drops or solid particles varies greatly depending on the class of materials, the state to which those materials have been exposed (i.e., thermal history, previous stresses in the material, surface treatments) and the environmental parameters associated with the erosion process such as impact velocity, impact angle, particle type and size, and coupled effects like ablation or corrosion.

1. LIQUID IMPACT

Categorization of the types of response of materials to liquid impact is shown in Table 1 as adapted from Adler (Reference 1). The free fall category refers to falling rain, impacting porous soil and causing ground erosion. The subsonic, supersonic, and hypersonic velocity regimes refer to impact below the velocity of sound in air (up to approximately 342 m/s), between 342 m/s and the dilatational wave speed in the material, and velocities greater than the dilatational wave speed respectively. Accordingly, most materials being impacted are rigid and analyses have been developed. The brittle response is an elastic-brittle response and is representative of the erosion of ceramics, glasses, uncoated composite materials, and thermosetting plastics. Non-brittle refers to the response of ductile materials such as most metals and thermoplastic polymers. The layered designation is included because protective coatings of elastomeric polymers, thin ceramics and metals over plastics and composites, and metal facings over other metal substrates have been successful in combatting erosion on aircraft radome and composite structures, composite missile radomes, and for steam turbine blade protection. The response of these layered materials is a function of the impedance match between coating and substrate, the degree of adhesion of the coating, and the impact conditions.

The composite material response is designated separately, although relatively little exists in the ability to analyze and design reinforced composites for improved erosion performance, because these materials are becoming more widely used for structural application when erosion is a major concern. Principal attempts to construct composite materials have concentrated on the design of carbon-carbon graphitic materials for re-entry vehicle thermal protection (Reference 2).

2. MODES OF LIQUID IMPACT DAMAGE

The response of nominally brittle materials to liquid impact is cracking of the surface due to the direct deformation impact loading on the surface. This cracking is typically in the form of disconnected annular ring segments which eventually intersect under continued impingement and result in chips of material being removed. Eventually large scale surface roughening and total original surface removal will occur. If the impact velocity is great enough, individual drops will cause massive fracture. A schematic of the damage modes in brittle materials due to liquid drop impact is shown in Figure 1 (Reference 3).

In porous ceramic materials such as reaction-sintered silicon nitride, the porosity provides a means of reducing crack propagation to prevent catastrophic fracture which can occur in denser ceramics.

The annular cracking which occurs in chalcogenide infrared windows such as zinc sulfide and zinc selenide can result in a loss of transmission through the window due to diffraction and absorption of the energy. However, this loss of transmission can occur when the material surface is not severely damaged or when material weight loss has not begun; it is caused by the in-depth propagation and intersection of droplet impact-caused ring fractures (Reference 4).

The erosion of thermosetting polymers in bulk form or as matrix resins in laminated or chopped fiber-reinforced composites takes the form of chunking on the surface. This breakage of the resin causes fibers (individually or as cloth in a laminate) to be partially exposed; subsequent impacts of droplets and the lateral outflow from these droplets

interact with these fibers causing column buckling or bending with fracture and removal.

The erosion of ductile materials such as metals and thermoplastic polymers assumes the form of initial surface depressions with upraised edges. These edges are susceptible to the lateral outflow jetting from the impacting drop leading to erosion pit nucleation. The depressions themselves are sites of local stress concentration but do not contribute to material removal (Reference 1).

By contrast, erosion pit nucleation exhibits a different sequence in Haynes alloy Stellite 6-B, which has been widely used as a remedy and, in fact, is the state-of-the-art for steam turbine blade erosion protection (Reference 5). In the wrought condition, this alloy contains 10 volume percent dispersion of coarse iron carbide in an alloyed cobalt matrix. Carbide/matrix cracking along with cracking of slip lines in the matrix is the initial damage followed by subsequent metal removal due to carbide particle ejection caused by lateral outflow. These carbide removal sites then act as erosion pit nucleation sites.

A major contribution to the material removal process is the repeated loadings of the surface during multiple impacts. At least three explanations have evolved to explain the removal sequence. One explanation finds a correspondence between erosion and fatigue in metals; some experimental evidence exists in the appearance of eroded samples (Reference 6). A fatigue theory has been developed by Springer (Reference 7) which will be discussed in a later section.

In experiments on titanium-6Al-4V alloy, Adler and Vyhna1 (Reference 8) found that the material removal was caused by a tunneling phenomenon due to hydraulic penetration and surface upheaval of regions which had been undermined by joining of cracks which originated at erosion pits. These tests were for water drop impacts with an imposed pressure of one half the yield strength of the alloy.

By contrast, Rieger (Reference 9) attributes the material removal to plastic deformation resulting in intense local concentrations of crystalline dislocations such that the internal stresses in these concentrated dislocation areas exceed the fracture strength forming a crack. The extension and joining of these cracks results in mass loss.

As described in the preceding paragraphs, the mechanisms of material removal even in nominally ductile metals are numerous and depend upon the microstructure of the alloy. The general form of the erosion and erosion rate as a function of exposure is shown in Figure 2 (Reference 1). The periods as labeled in this figure reflect the common terminology used to describe different portions of the process (Reference 10). The incubation period in which no mass loss occurs, although the damage may be accumulating in the form of surface deformation, cracking, or fatigue is perhaps a characteristic of individual materials and is often used as a measure of erosion performance. The slope of the erosion vs time curve is also an important characteristic of materials. Theories have been developed which attempt to incorporate these features (References 7, 11, 12) and will be discussed in Section III.

Obviously, at very high impact velocities where each drop impact may cause material removal, the existence of incubation periods and changing erosion rates is not descriptive of the phenomena which occur.

The deformation modes and erosion mechanisms for polymeric materials caused by liquid impact have been identified by Adler and Hooker (Reference 12) and Schmitt (Reference 13). At subsonic velocities, most polymeric materials such as polycarbonate, polysulfone, and polymethylmethacrylate exhibit ring crack formation after drop impact but maintain a central region of undamaged material within this ring crack. The damage was concentrated in an annular zone associated with the region of maximum pressure from the drop impact.

The response of polymeric materials has been found to be different for thermoplastics such as polyethylene, nylon, polyphenylene oxide, and thermosets such as polyimides and epoxies. In these materials, the

addition of reinforcement to thermoplastics is detrimental to erosion performance because the fibers tend to break out under repeated impingement enhancing the mass loss. The thermosetting polymers benefit by reinforcement because the fibers reduce massive breakage and chunking of the brittle resin (Reference 14).

Recent studies by Gorham, Matthewson and Field (Reference 15) on reinforced and non-reinforced thermosetting and thermoplastic polymers have confirmed the above conclusions and determined that absorption of the impact energy by ductile failure in composites is desirable and the thermoplastics provide this.

The liquid impact erosion of elastomeric coatings has been extensively studied (References 16, 17, 18) and much development of polyurethane and fluorocarbon coatings has been conducted for protection of aircraft radomes and composite surfaces. The polyurethane coatings developed in 1966-69 replaced neoprene coatings which has been in use since the early 1950's. The fluorocarbons have been developed since 1972 for higher temperature applications. Development has been empirically based through extensive screening on rotating arm rain erosion simulation apparatus (Reference 19).

The neoprene coatings erode under liquid impact by a gradual roughening of the surface and eventual adhesion loss as the coating is loosened from the surface and torn by subsequent impact. The polyurethane coating fails by an isolated hole typically the size of a pencil point which fails to the substrate while the surrounding area of the coating remains intact, looking as though it has not been exposed. The fluorocarbon coating erodes by chunking of pieces from its surface and gradual wearing away until the substrate is exposed.

Other brittle polymeric coatings such as epoxies, silicones, polyesters, acrylics, and nonelastomeric polyurethanes fail by brittle rupture and/or spall of the coating very rapidly upon impact. All of the above behavior applies to low velocity impact conditions.

3. SOLID IMPACTS ON DUCTILE METALS

Removal of material by solid particle impact is perhaps the most pervasive of the erosion processes due to growing utilization of coal in fine particulate form in energy conversion plants, other combustion product particulates in flue gases in these plants, solid impact in jet engines and on helicopter rotor blades, and even in large scale turbines due to spall and subsequent impact of oxide particles on downstream blades and surfaces. A major National Materials Advisory Board study (Reference 20) has addressed the erosion question of the energy conversion processes and the reader is referred to it.

As is the case with liquid impact, several mechanisms are recognized as occurring depending upon the ductility or brittleness of the material being impacted.

A schematic of the features of erosion on ductile and brittle materials as a function of angle is shown in Figure 3 (Reference 21). The understanding of the mechanisms has been discussed in three recent papers and will be summarized here (References 22, 23, 24).

The elements of ductile metal erosion by solid particles at low to moderate velocities parallel those of liquid impact in that surface deformation without mass loss initially occurs followed by a removal process which has been the subject of much controversy and theory development.

For ductile metals, the maximum erosion occurs at an impingement angle of approximately 20 degrees (normal impact being 90 degrees). This behavior was originally modeled by Finnie and co-workers (Reference 22) by considering the abrasive cutting by a rigid angular particle in the surface of a ductile metal. A constant ratio of normal to tangential force is assumed with a force vector of constant direction. In this theory, the volume of material removed is a function of the mass impacting, velocity-of-impact squared, the impact angle, and inversely proportional to the horizontal component of flow pressure which is related to the

hardness between the particle and the material. This approach does not describe the erosion of ductile materials at high impingement angles (greater than 45 degrees) adequately.

A classic analysis by Bitter (Reference 25) described the erosion process as consisting of two simultaneous processes: cutting wear which dominates at low angles, and deformation wear which dominates at high angles. This work is often referenced in erosion literature.

Tilly and co-workers (Reference 26) described a two-stage process whereby particles, instead of being rigid, produce erosion by impact and then fragment to produce additional erosion. The fragmentation and outward flow of particle fragments cause the erosion at 90 degrees, according to Tilly et al, and can be used to explain the velocity dependence of erosion as greater than two as observed experimentally. Numerous investigations (Reference 24), for example, have shown velocity exponents of 2.3 and greater and increased fragmentation at higher velocities was used to explain this. This fragmentation included the particle size effect which had been observed experimentally since larger particles would be more prone to fragment and produce additional damage than small ones.

Smeltzer, Gulden and Compton (Reference 27) attribute the erosion mechanism to localized melting during impact with attachment of surface material to impacting particles. Although experimental evidence provides some basis for these conclusions, the theory has not been widely accepted.

An energy balance between the kinetic energy of the particle and the work expended during indentation forms the basis for the model of Sheldon and Kanhere (Reference 28) which relates the erosion resistance of the material (at 90 degrees impact) to the Vickers' hardness to the $2/3$ power.

Experiments by Hutchings using idealized rectangular plates and spherical particles have identified three mechanisms which are operative in ductile metal erosion (Reference 22). These are: (1) Plowing deformation resulting in a raised lip on the trailing edge of the crater which was original material pushed up by the rounded surface of a particle; (2) Type I cutting which results in a triangular indentation which is pushed up into a large lip at the exit end of the crater; and (3) Type II cutting in which the plate rotates backward upon impact resulting in a smooth shallow crater from which all material is removed. Type I cutting is observed on plates with a negative rake angle which rotate forward in impact (Figure 4). A plate with rake angles between 0 and -17 degrees exhibits Type II cutting behavior. Examples of these three craters are shown in Figures 5a, 5b, and 5c.

Analyses of the above craters show crater volumes proportional to the energy lost by the projectile in both plowing and Type I cutting; however, velocity exponents are 2.4 for plowing and 2.0 for Type I cutting. The assumption which contrasts Hutching's analysis with that of Finnie is a constant yield pressure acting over the area of the particle which is plastically deforming the substrate, leading to a continually changing direction of the force vector during impact (Reference 23).

Normal (90-degree) impact erosion of ductile metals is attributed to a wide variety of mechanisms including work hardening and embrittlement, fracture of solid particles on impact with subsequent outward flow of fragments, extrusion of surface, delamination of subsurface material, melting, and low cycle fatigue. Finnie (Reference 22) describes the condition of the surface as an extrusion of material as a result of continuous pounding of the surface until ductile fracture occurs. This removed material is flake-like in nature. Microscopic examinations eliminate embrittlement, fragmentation of particles, and melting as mechanisms with extrusion, low cycle fatigue, and delamination wear remaining as possible explanations.

The role of particle embedment on the steady state erosion of ductile materials is beginning to be explored. Ives and Ruff (Reference 21) have found the embedded particles to be much smaller than the incident particles resulting from fragmentation upon collision. The resulting mixed layer of deformed metal and embedded fragments is what is impacted and removed by subsequent impacts.

The role of temperature in the ductile erosion process is not well understood because much of the past research has concentrated on room temperature testing. However, considerable emphasis is now being placed on elevated temperature erosive processes (Reference 20).

Correlations between thermal properties of materials and erosion rates have been developed by Ascarelli (Reference 29) for pure metals with the product of the linear thermal expansion co-efficient, which is the temperature rise required for melting and the bulk modulus of the metal. Other correlations also exist with the following properties: (1) product of density, specific heat and temperature rise required for melting, (2) melting point, and (3) the cube root of the mean molecular weight divided by the thermal conductivity, the enthalpy of melting, the melting temperature, and the cube root of the material density. It is not clear that thermal properties really have significant influence on erosion resistance of metals.

Strain rate properties appear to have very significant influence on the erosion resistance of materials since the strain rates are typically 10^6 (Sec⁻¹) or greater. Conventional materials properties are measured at low strain rates and hence poor correlation between erosion rates and conventional properties is found.

4. SOLID IMPACT ON BRITTLE MATERIALS

In contrast to the erosion of ductile materials where erosion is maximum at an impingement angle of 20 to 30 degrees, the erosion of brittle materials is a maximum at 90 degrees (normal impact). Figure 2 gives a schematic representation of typical brittle material erosion as a function of angle.

The erosion of ceramics, glasses, and thermosetting polymer matrices in composite materials by solid impact is receiving increased emphasis because ceramics and composites are being employed for engine applications where dust ingestion is a concern and ceramics are being employed as refractory liners in energy conversion equipment. Glasses and ceramics are utilized as optical domes and radomes of tactical missiles where solid particle impact during captive carry on the aircraft is a concern. The use of fiber-reinforced composites on helicopter rotor blades which are operated in sandy or dusty environments has not only caused study of the erosion behavior of these materials but has resulted in the development of state-of-the-art protective coatings schemes including electroplated nickel and polyurethane for erosion protection. A similar situation exists for composite jet engine blades and vanes which must also be protected.

The impact of solid particles on brittle materials has been analyzed using the Hertzian theory of impact for the collision of elastic bodies in an elastic half-space (References 1, 23, 30, 31). Although the quasi-static stress distributions from this analysis are not accurate at moderate impact velocities, considerably wider applicability of the estimates for sizes of contact zones and durations of impact has been found than would be expected based on the assumptions in the theory.

The cone and ring cracks which form in a Hertzian impact are presumed to intersect, and with a sufficient number of them, mass loss will occur by breakout of chunks of material. Radial cracking occurs and results in strength degradation. This process has been studied and confirmed experimentally by Adler (Reference 30) who also expanded the analysis. However, the complexity of the process has prevented complete definition.

An alternative theory to the Hertzian analysis is based upon dynamic plastic indentation which has the features of plastic deformation of the contact area between the particle and the target material, radial cracks propagating outward from the contact zone, and lateral cracks that initiate beneath the contact zone and propagate between the radial cracks on planes nearly parallel to the surface (Reference 32).

The model predicts an erosion volume loss dependence of velocity to the 2.5 power and particle radius to the fourth power. Experimental data agreement was reasonable for silicon carbide particles impacting hot pressed silicon nitride and for quartz on hot pressed magnesium fluoride but other particle/target combinations did not agree as well (Reference 33).

It is evident that the fracture threshold depends on target parameters such as the surface flaw size distribution, fracture toughness and elastic wave speed (Reference 34). However, the equivalent parameters involved in the erosion process have not yet been seriously explored. Intuitively, it would be anticipated that the toughness is very important, but the roles of microstructure (grain, pore size, and morphology) and the elastic properties cannot be meaningfully presupposed (Reference 20).

Although ceramic materials will normally be used for high temperature applications either as primary structures, rotating components, or protective liners, very little solid particle, erosion, or impact data at elevated temperatures exist in the literature for materials of interest. Changes in the plastic deformation behavior of these materials at elevated temperatures, due to increasing dislocation mobilities, would change their erosion characteristics.

Research that has been done (Reference 35) has identified plastic material removal processes in ceramics at elevated temperatures. These processes exhibit a maximum erosion rate at incidence angles of 15 to 20 degrees and a functional dependence on the inverse of the target hardness. Localized fracture is a more common erosion mechanism with a dependence to some extent on the inverse of the fracture toughness and the hardness.

Recent work on predictions of crack formation and growth (as a function of critical flaw size), strength degradation, crack size, and lateral crack depths is reviewed by Ruff and Wiederhorn (Reference 35) for single particle impacts.

AFML-TR-79-4122

Solid particle erosion of bulk polymeric materials has received virtually no emphasis because no applications are extant where solid impact is a problem.

SECTION III

EROSION PREDICTION TECHNIQUES

Predictive techniques for estimating the life of components subject to erosive environments are in a preliminary stage of development because of the complexity of the processes which have been described in the preceding sections. These predictive techniques are required to gauge the expected performance of components and systems during single and multiple flights in the case of aircraft, during operation of large steam turbines for thousands of hours, and for the prediction of erosion on scale-up to operating size in energy conversion plants. Most laboratory erosion tests are conducted under accelerated conditions and methods for translating those results to real life equipment prediction are required; particularly in coupled environments where one or more, or perhaps all, environmental effects are accelerated. Accurate prediction techniques depend upon a better understanding of the individual phenomenological effects and the ways to couple them.

In view of the inadequate understanding that exists for translating single particle impacts to multiple particle erosion, it should be no surprise that predictive techniques are in an early stage of development even without various additional effects coupled in. Two theories for liquid impact erosion will be described and their inadequacies are to be expected considering the state-of-the-art. Similarly, the solid particle erosion theories which have already been discussed in connection with the modes of materials damage will be summarized.

1. THIRUVENGADAM'S THEORY OF LIQUID IMPACT EROSION

Thiruvengadam (References 11, 36) developed the concept of erosion strength S_e , which was defined as the energy-absorbing capacity of the material per unit volume under the action of erosive forces. In his model, the erosion process is controlled by two opposing phenomena, the time-dependent efficiency of absorption of impact energy by the target material, and the attenuation of the impact pressure due to changing surface topography as the target material erodes.

The intensity of a single drop impact is defined by Thiruvengadam as:

$$I_c = \frac{P_w^2}{\rho_w c_w} \quad (1)$$

where I_c is intensity

P_w is pressure imparted to surface by the liquid impact
 ρ_w is density of water
 c_w is compressional wave velocity for water

The attenuation of the intensity of impact, I_1 is assumed to be inversely proportional to the perpendicular distance to the impact plane raised to the n^{th} power.

$$I_1 = \left(\frac{A}{R+R_f} \right)^n I_c \quad (2)$$

Where

I_1 = attenuated intensity
 A = proportionality constant
 R = mean depth of erosion from original surface
 R_f = thickness of liquid layer on surface

The intensity of erosion which is defined as the power absorbed by a unit eroded area of the material is designated I_e .

$$I_e = S_e \frac{dR}{dT} \quad (3)$$

The intensity of erosion is assumed proportional to the impact intensity:

$$I_e = \eta I_1 \quad (4)$$

Where $\eta = \eta(t)$ is a time dependent material property governing the efficiency of energy absorption.

Equations 2, 3, and 4 are then used by Thiruvengadam (Reference 36) to derive the normalized form of the differential equation governing the erosion intensity.

$$\frac{d\bar{I}}{d\tau} + \bar{k} \left(\frac{\bar{I} (2m+1)/m}{\bar{n}} \right) - \frac{\bar{I}}{\bar{n}} \frac{d\bar{n}}{d\tau} = 0 \quad (5)$$

This equation has been normalized with respect to the maximum intensity of I_{max} and the time τ_1 at which the maximum occurs (Figure 2). These parameters are:

$$\tau = \frac{t}{\tau_1}, \quad \bar{I} = \frac{I}{I_{max}}, \quad \bar{n} = \frac{n}{n_1}, \quad \bar{k} = \frac{dn}{d\tau} \Big|_{\tau=1}$$

The normalized differential equation can be solved, thus:

$$\bar{I} = \frac{n}{[1 + \bar{k} \frac{n+1}{n} \int_1^{\tau} n^{n/n+1} nd\tau]} \quad (6)$$

Values of $n = 2$ based on shock attenuation in underwater explosions and $\eta(\tau) = 1 - \exp(-\tau^\alpha)$, a Weibull distribution based on analogy between the repetitive loading in an erosive environment and fatigue of metals under repeated loading cycles, the intensity of I as a function of τ can be calculated. The Weibull shape parameter, α_j is a function of the magnitude of the applied stress and the material itself.

Adler (Reference 1) has recently pointed out that Thiruvengadam's theory is dependent upon the presence of a layer of liquid on the material which attenuates the loading pulse as it travels through the layer. The parameter, n , in Equations 5 and 6 is intimately related to this theory and it has no physical meaning in most liquid drop situations since liquid layers, either are negligibly thin or nonexistent due to aerodynamic flow considerations in most erosive applications of interest.

Thiruvengadam's model has been generalized to cover all liquid drop impact cases and a nomograph was generated based on cavitation data which enabled one to estimate erosion strength and life of materials as a function of the erosion intensity in a particular application (Figure 6). However, it would appear that extension of the theory to liquid drop impact requires assumptions which are removed from reality.

2. SPRINGER'S THEORY OF LIQUID IMPACT EROSION

Springer, et al (References 7, 37, 38, 39, 40), organized erosion data from the literature and developed a theory of erosion based upon fatigue concepts. This theory which was developed under Air Force sponsorship was extended from monolithic materials (Reference 37), to analyze erosion of composite materials (Reference 38), coated materials (Reference 39) and electromagnetic transmission losses in transparent materials (Reference 40).

The model is based upon the assumption that the incubation period, acceleration period, and maximum rate periods of the characteristic erosion curve as shown in Figure 2 can be represented by the linear relationship:

$$M^* = \alpha^* (N^* - N_i^*) \quad (7)$$

where

M^* is dimensionless mass loss
 α^* is dimensionless rate of mass loss
 N^* is dimensionless number of impacts per site
 N_i^* is dimensionless number of impacts corresponding to the incubation period

This representation is shown in Figures 7a and 7b.

Based upon the use of Miner's rule as it applies to the torsion and bending fatigue failure of ductile metals and extending that analysis to the stresses induced by random drop impact loading on the surface, Springer derives the expression for impacts in the incubation period as follows:

$$N_i^* = a_1 \left(\frac{S}{P}\right)^{a_2} \quad (8)$$

where a_1 and a_2 are constants

p is the interfacial pressure due to a water drop impact

and

$$S = \frac{4\sigma_u (b-1)}{(1-2\nu) \left[1 - \left(\frac{\sigma_I}{\sigma_u}\right)^{b-1} \right]} \quad (9)$$

where

ν is Poisson's ratio

σ_u is the ultimate tensile stress

σ_I is the endurance limit

and b is derived from $S - N$ curve in fatigue, $b = \frac{b_2^2}{\log_{10} \left(\frac{\sigma_u}{\sigma_I}\right)}$

A plot of existing data on incubation period versus the ratio of S over P is shown in Figure 8. The values of n_i were obtained from the erosion tests and the values of S and P were calculated from the impact conditions (drop size, velocity and impact angle) and the materials properties (σ_u , σ_I , b_2 , ρ , E , and ν).

$\left(\frac{\sigma_I}{\sigma_u}\right)^{b-1}$ is assumed to be $\ll 1$
in these calculations.

A least squares fit to the data becomes:

$$N_i^* = 7 \times 10^{-6} \left(\frac{S}{P}\right)^{5.7} \quad (10)$$

which is the solid line in Figure 8.

A comparison of the model with single point data (total mass loss is given at only one instant in time) is made by rewriting Equation 7 in the form:

$$\frac{M^*}{\alpha} = N^* - N_i^* \quad (11)$$

This comparison is presented in Figure 9 and agreement is reasonable despite the assumptions which were made. It is pointed out that the model as described is limited to $N_i^* > 1$ since fatigue requires multiple impact and $\frac{S}{P} > 8$ as the lower limit for the impact conditions. The upper limit requires that the mass loss vary linearly with n and typically, $n^* < 3n_i^*$.

Adler (Reference 1) has described the nature of the assumptions and what he believes the limitations of the Springer model are. Among these are arbitrary selection of a constant value of b which is applied to all metals, polymers, and ceramics. This and neglecting σ_u/σ_I removes the dependence on the fatigue curve. The ratio of S/P becomes the ratio of the static ultimate tensile stress to the radial tensile stress component. The material constants required are then the ultimate tensile strength and Poisson's ratio. Thus the curves become a simple empirical fit to the incubation impacts N_i^* versus ratio of S/P and m^*/α^* versus $n^* - n_i^*$ in Adler's view.

3. BRITTLE MATERIAL - LIQUID IMPACT THEORIES

Attempts to model the erosion of brittle materials have been made by Adler (Reference 41) and Engel (Reference 42). Adler's approach was based upon erosion pit nucleation and growth. While this approach is physically realistic in representing the erosion process, it has been impossible to specify the explicit forms of the nuclear and growth rate functions. Thus, while a general framework has been formulated, it has not yet been implemented.

A statistically based analytical approach for liquid drop erosion of brittle materials was constructed by Engel and is a complex conceptual model which makes numerous approximations to the physical processes in erosion. However, model development was never completed due to retirement of the author.

4. HERTZIAN IMPACT THEORIES

Hertz (Reference 43) described the collision of a deformable sphere with a deformable target for elastic materials. The time-dependent radius of the contact area is:

$$a(t) = a_1 \sin^{1/2} \left(\frac{Kt}{T} \right) \quad (12)$$

where a_1 is $K^{1/5} r V_0^{2/5}$ = maximum contact radius

T is $2.943 K^{2/5} r V_0^{-1/5}$ = duration of the bodies on contact

K is $1.25 \pi \rho_1 \left[\frac{1}{\rho_1 c_1^2} + \frac{1}{\rho_2 c_2^2} \right]$ = elastic properties of impacting bodies

ρ_1, ρ_2 are densities of sphere and target

c_1, c_2 are elastic wave velocities for sphere and target respectively.

The elastic wave velocity may be calculated:

$$c^2 = \frac{1}{\rho} \frac{E}{(1 - \nu^2)} \quad (13)$$

where E is Young's Modulus

ν is Poisson's ratio

For a deformable sphere impacting a rigid body, Equation 12 becomes:

$$a(t) = \left(\frac{5}{4} \pi \right)^{1/5} r \left(\frac{V_0}{c_1} \right) \sin^{1/2} \left[\frac{\pi}{5.7} \left(\frac{c_1}{V_0} \right)^{4/5} \left(\frac{V_0 t}{r} \right) \right] \quad (14)$$

When the relative velocity between the two colliding bodies is zero,

$$a(t) = a_1 = \left(\frac{5}{4} \pi \right)^{1/5} r \left(\frac{V_0}{c_1} \right)^{2/5} \quad \text{at time } t = \frac{T}{2} \quad (15)$$

The maximum contact radius is determined by the elastic wave speed c , which is a function of the elastic properties as shown in Equation 13. For a rigid sphere, which is an idealized particle in solid erosion, c_1 approaches infinity and a_1 approaches zero.

The form of the pressure distribution between an impacting liquid drop and a solid surface is different from that of a solid body impacting that surface. The solid body impact pressure will be a Hertzian paraboloid distribution with a maximum at the center (axis of symmetry of body) (See Reference 2 for a thorough discussion).

$$P = P_{\max} \sqrt{1 - \frac{r^2}{a^2}} \quad (16)$$

By contrast, the form of the liquid pressure distribution is not known exactly. Figure 10 illustrates two experimentally measured and two numerical code calculations of that pressure distribution under liquid drop.

The magnitude of the drop impact pressure is calculated from the water hammer pressures as follows:

$$P_W = \rho_W C_W V_0 \quad (17)$$

Where

- ρ_W is density of liquid
- C_W is acoustic wave velocity in the liquid
- V_0 is the liquid impact velocity

Taking compressibility of the target into account results in:

$$P_W = \frac{\rho_W C_W V_0}{1 + \frac{\rho_W C_W}{\rho_t C_t}} \quad (18)$$

where ρ_t and C_t are the density and compressional wave velocity in the target material.

Engel (Reference 44) also modeled the impact of a water drop on a rigid surface and obtained the expression:

$$P_W = \frac{\alpha}{2} \rho_W C_W V_0 \quad (19)$$

where $\alpha/2$ results from the spherical shape of the water drop.

In the expression, α was a reduction factor for the particle velocity in the compressed zone of liquid as the compression wave traverses the drop (Reference 45). In this analysis, P_W is the average pressure over the circle of contact at the time the peak pressure is reached.

Considerable analysis and effort in calculating and measuring the value of P_W have occurred in the erosion literature (References 46, 47, 48, 49). These results are summarized in Figure 10 (References 50, 51).

5. BRITTLE MATERIAL MODELS

The two models which were previously discussed in Section II for brittle materials are based upon Hertzian cracking, crack propagation and chipping and one based on the contribution of plastic deformation to crack formation and surface chipping. These are discussed in Reference 35 at length and the reader is referred to that publication.

The elastic plastic theory of Evans et al (Reference 32) predicts the erosion rate as follows:

$$V = V_0^{19/6} r^{11/3} \rho^{19/12} K_C^{-4/3} H^{-1/4} \quad (20)$$

where V is volume lost per impact

- V_0 is impact velocity
- r is particle radius
- ρ is particle density
- K_C is stress intensity factor
- H is dynamic hardness

This equation predicts exponents on the equation for mass loss ratio (mass eroded/mass impacted):

$$W = k_1 r^a v^b \quad (21)$$

of $a = 3.7$ and $b = 3.2$ which are in reasonable agreement with experimental data.

6. EMPIRICAL MODELS

While elements of the fundamentals of impact processes are included in all of the analyses previously described, their state of development is such that empirical data fitting has been used for years in erosion for performance prediction. Initially this was because the processes were so complex that an appropriate analytical framework did not exist. As this understanding grew and the true complexities emerged, it became expedient from time and cost standpoints to use empirical models.

Erosion problem areas where such models have found particular use are those of moderate velocity tactical missile radome, very high velocity reentry vehicle nosetips and heat shields, and gas turbine blades (References 2, 52, 53).

Schmitt has utilized equations of the form:

$$\text{MDPR} = K V^\alpha \sin^\beta \theta \quad (22)$$

where MDPR is mean depth of penetration rate

K is a constant

V is velocity

θ is impact angle

α, β are empirically determined exponents

For uncoated two-dimensionally reinforced composite materials, a sine squared expression best fit the data in a velocity regime from 1500 to 5500 feet per second. For three-dimensionally reinforced composites, a sine cubed expression provided the best fit (Reference 2). Monolithic ceramics erosion was described by the following expression:

$$\text{MDPR} \sin \theta = K (V \sin \theta)^\alpha \quad (23)$$

In the expressions for ceramics, laminates and bulk plastics, the velocity was typically the fifth to seventh power. This very high dependence upon impact velocity for liquid impact erosion in a moderate velocity regime has been confirmed by numerous experiments (References 54, 55).

For the carbon-carbon composites and graphites, Equation 22 with $\beta = 3$, provided the best fit for the data in the speed regime 4000 to 5500 feet per second. Table 3 summarizes these data (Reference 2).

Extrapolation of rain erosion data from subsonic to supersonic to hypersonic velocities has been difficult because of the changes in response of the materials in the various velocity/temperature coupled environments. Thus the correlations of data such as those of Schmitt have found only limited application (Reference 56) and only then in the velocity regime in which they were obtained.

SECTION IV
EROSION DATA SOURCES

1. LIQUID IMPACT

The rain erosion data are concentrated in the proceedings of the four International Erosion Conferences (References 6, 8, 9, 13) and the Special Technical Publications from symposia sponsored by ASTM Committee G-2 on Erosion and Wear (References 2, 5, 37, 52). An excellent compilation of multiple liquid impact erosion data may be found in Tables D-1 and D-2 of Reference 7 along with specific references to the original reports in which these data may be found. Included are many technical reports which are otherwise seldom cited.

The liquid impact erosion data are often presented in the form of curves of weight loss or erosion depth as a function of time of exposure. Examples are shown in Figures 11 and 12 for materials exposed at 410 m/s and a rain concentration of 10^{-5} g/m³ in the Dornier Systems GmbH rotating arm multiple impact facility (Reference 54).

The comparative behavior of nonmetallic materials which have been exposed to identical velocity/impact angle/erosive conditions in the AFML rotating arm rain erosion simulation apparatus at 223 m/s is described in References 14, 57, and 58 and at speeds of 1600 m/s from the Holloman rocket sled rain simulation in References 2, 52, 59 and 60.

Erosion data on metallic materials may be found in the Erosion Conference proceedings and in the Special Technical Publications previously referenced. An important reference report on turbine blade materials liquid impact erosion which summarized much of the existing understanding and data on these materials may be found in Reference 61. Other especially important sources of data on turbine materials are References 62 and 63.

The comparative behavior of brittle materials is described for rotating arm tests in References 4, 64, 65, and 66. In general, the velocity exponents for glasses and ceramics are considerably higher

(up to 13) than for metals or plastics (typically 5 to 7). Most brittle materials have criteria for damage other than weight loss; for example, reduction in transmission through optical materials or catastrophic fracture in supersonic radome ceramics.

2. SOLID IMPACT

The accessible data base for solid particle impact erosion of materials is quite limited because much of the early work on metals was considered proprietary to jet engine manufacturers and there has not been extensive research on ceramics. It is only with the current emphasis on erosion in energy conversion systems that widely available data are becoming disseminated.

A recent comprehensive screening program was undertaken by Hansen (Reference 67) using an S. S. White Abrasive Unit for impacting over 200 materials with 27 micron alumina particles at velocities of 170 m/s at room temperature (20°C) and elevated (700°C) temperatures. Impingement angle was 90 degrees. Figures 13 and 14, which are taken from Reference 67, show the relative ranking of metals and ceramics normalized to the resistance of Haynes Stellite 6B, which is a widely used erosion resistant alloy. Similar rankings are shown in Tables 4 and 5 which identify the materials.

Conclusions from these data are that improvement over Stellite 6B was at best 30 percent for any of the metals either at room temperature or 700°C. Furthermore, similar rankings were obtained with increased erosion volumes at a 20 degree impingement angle where the erosion would be maximized in ductile materials. Molybdenum and tungsten were exceptions with improved resistance of a factor of two or more under all conditions.

The ceramic materials (Figure 14) and some cermets (Figure 15) exhibited relative performance which varied from several times as erosion prone as Stellite 6B to a factor of three to five better at room temperature. This relative improvement was somewhat greater at 700°C, as might be expected. Several materials such as cubic boron nitride and diamond

exhibited no weight loss at all at either temperature. More practical ceramics such as silicon nitride, silicon carbide, zirconium diboride-tungsten carbide-alumina mixtures and boron carbide, which were hot pressed or pressed and sintered, gave improved erosion resistance compared to the Stellite 6B. The ceramic results were very dependent on density and porosity.

Excellent results were also obtained with coatings of chemical vapor deposited silicon carbide, diffused tungsten carbide and especially electrodeposited titanium diboride. Results are summarized in Tables 6 and 7 for these coatings. Thicknesses of 50 to 80 microns were required to achieve erosion resistance and the 700°C tests demonstrated the need for thermal expansion match between the coating and substrate.

Data on metallic engine alloys including 2024 aluminum, titanium-6Al-4V, 410 stainless steel and 17-7PH steel may be found in References 27 and 68. A variety of dust types (including alumina, silica-rich Arizona Road Dust, and laetrite particles) was employed.

Tilly and Sage (Reference 69) obtained data on metal, plastics and ceramics as a function of impacting velocity, particle size and type and impingement angle. Similar data were obtained by Sheldon (Reference 70) on ceramics and metals.

The recent work of Tabakoff and co-workers (References 71, 72) have included the effects of aerodynamic flow and temperature with solid particle erosion of gas turbine materials. They have determined a velocity dependence of 3.8 for the exponent which is considerably greater than earlier research had indicated.

SECTION V
MATERIALS PROPERTIES EFFECTS

Materials developers concerned with combatting erosion by developing materials with improved liquid and solid particle erosion resistance have long been searching for appropriate materials properties with which to correlate erosion resistance. The hope is to discover a simple materials property or group of properties to maximize to provide this improvement. To date, no satisfactory simple correlation has been found because most materials hardness or strength properties are measured at loading rates which are not representative of those in impact situations and hence are not indicative of the controlling behavior of the material.

1. METALS

Attempts to provide correlations with material hardness (References 22, 28, for example) have been at best moderately successful. Changes in the condition of the surface under repeated impact have the effect of work hardening or deforming the surface so that the original surface hardness has little controlling effect on the erosion process. See Reference 73 for a discussion.

Numerous correlations have been attempted with strain energy properties and some success has been achieved by Thiruvengadam (Reference 74), Hobbs (Reference 75) and others. However, there are exceptions to this, particularly with Stellite 6B, which has exceptional erosion resistance but only moderate strain energy based on tensile tests.

Gould (Reference 76) demonstrated that the exceptional erosion resistance of Stellite 6B cobalt-chromium alloy was due to the ability of its cobalt base matrix to absorb energy in undergoing a strain-induced phase transformation from face centered cubic to hexagonal close packed structure. The erosion resistance was also shown to be independent of hardness or grain size. Therefore, it appears that the strain energy properties provide at least one clue to developing improved materials.

Other correlations (Reference 29) with thermal properties such as thermal expansion coefficients, specific heat, temperature rise required for melting, melting point, etc. have been developed, but a clear cut correlation is not evident.

2. POLYMERS

Development of polymeric coatings, composites and bulk plastics with erosion resistance has concentrated on elastomeric coatings for rain erosion resistance and assessment of plastics behavior. Correlations with properties have been minimal because the rotating arm apparatus (Figure 6) provides a direct simulation of the actual rain encounter (except for centrifugal force effects) and success has been achieved in improved polyurethane and fluorocarbon coatings by doing ranking and development with the rotating arm. Correlations between rotating arm ranking and actual flight exposures have been obtained (Reference 77) and the performance of improved materials in actual service has further confirmed the use of this apparatus (Reference 78).

Conn and Thiruvengadam (Reference 79) utilized a split Hopkinson pressure bar apparatus to study the dynamic stress-strain characteristics of elastomeric rain erosion resistant coatings. This apparatus provided strain rates of 10^4 sec⁻¹ which approached the loading rate in an actual drop impact. Considerable controversy ensued over utilization of the apparatus because of the assumptions associated with uniaxial stress for a drop impact on which its use was predicated (Reference 13). No direct correlation between strain rate properties and erosion resistance was determined in these studies.

Oberst (Reference 80) described the erosion of bulk polymers as related to their notch impact strength and found a general correlation between the two. However, scatter in values of notch impact strength and other complications in the experiments (performed at Dornier) such as temperature rises prevented a definitive correlation.

3. CERAMICS

The plastic deformation observed in ceramics at elevated temperatures and/or low impact angles is particularly important and results in residual stresses which can cause crack formation and chipping (Reference 35). This behavior is governed by the dynamic hardness (hardnesses measured under impulse loading) and the critical stress intensity factor of the material. The ductile-to-brittle transition of ceramics is determined by the behavior of these variables as a function of temperature but tests have indicated the critical stress intensity factor of ceramics is not dependent on temperature. There is also indication that dynamic hardness may be independent at least for short times (less than 10^{-4} sec). The ability of the elastic-plastic theories to predict ceramics erosion indicates that the dynamic toughness which governs those elastic-plastic processes is a critical property for these materials.

The influence of density and porosity on the liquid impact erosion of reaction sintered silicon nitrides has been described by Schmitt (Reference 81). He determined that a tradeoff could be made between maximizing density/minimizing porosity (which resulted in minimum surface erosion and increased in-depth cracking) and intermediate density/porosity, where strength properties were sufficient for structural purposes and surface erosion was acceptably moderate while cracking was eliminated. It appears that for certain ceramics the porosity can be tailored to cause crack arrest in severe erosive exposures (in these tests, which were Mach 4 velocity rain impacts).

Other experiments by Schmitt (Reference 82) on most state-of-the-art ceramics showed that some monolithic materials (alumina, beryllia, hot pressed silicon nitride) which had extremely high strength properties would survive a 1600 m/s multiple impact exposure with no damage. Still others (Pyroceram, cordierite, slip cast fused silica) exhibited massive fracture, particularly at higher impact angles.

Thus, it can be concluded that for the above classes of materials, no simple set of materials properties can be optimized for erosion resistance. Dynamic properties at strain rates comparable to impact loading are the keys to erosion performance. For these reasons empirical determination of erosion resistance and extensive screening and relative ranking of materials have proven to be cost-effective ways of developing materials, particularly for multiple impact erosion environments. Studies of other properties which would be expected to influence erosion resistance such as grain orientation, size and toughness, have not been conducted as yet.

SECTION VI
MATERIALS TO RESIST EROSION

The resistance of materials to liquid drop and solid particle impact erosion has been determined experimentally with ranking of materials as a major output of these determinations. Due to the complexity of the erosive processes, particularly in multiple impingement, this approach has proven cost effective because actual field experience has confirmed the improved performance of these materials.

1. METALS

Liquid drop impact in large steam turbines led the manufacturers of such equipment to screen and rank metals for erosion resistance. Thin coatings were avoided because of very long life continuous operating conditions which dictated reliance on inherent materials characteristics rather than on a thin protective layer.

These screening tests led to the selection of Stellite 6B alloy applied as protective leading edge shields or as bulk material. Service experience proved that the Stellite 6B combatted the problem so effectively that the steam turbine manufacturers were able to de-emphasize research for new erosion resistant blade materials. A case history of this material development may be found in Reference 20.

For helicopter main rotor blades operating in dusty or sandy unimproved areas, the solid particle impact damage was sufficiently severe that dynamic operation of the blade became unstable due to pitting and roughness on the leading edge perturbing the aerodynamics. After considerable development, the use of electroplated nickel, which had been pioneered for liquid impact erosion protection by Weaver (Reference 83), was adopted for rotor blade protection. The nickel was applied either as an electroformed nickel sheath adhesively bonded, or fastened to the aluminum rotor blade, or plated onto a stainless steel sheath which was then fastened to the rotor leading edge.

This system or some variation of it is still the state-of-the-art for rotor blade erosion protection including that for advanced composite graphite epoxy or Kevlar-epoxy constructions. Because of weight requirements, the metal is used only on the high impact angle and severe exposure areas, while the remainder of the blade is coated with elastomeric polyurethane.

The polyurethane alone as a protective coating was investigated but did not provide sufficient long term resistance to severe particle impact environments; hence, it has only been used in low impact angle surfaces.

The selection of metals and metal alloys for gas turbine vanes and blades has traditionally been based on mechanical strength properties, fatigue resistance, and creep resistance in rotating dynamic environments. Tolerances are typically extremely tight and allowances for erosion protective measures are minimal. As a result, thin chemical vapor deposited or sputtered coatings have been investigated. Titanium carbon-nitride, titanium diboride, ferric boride, and other coatings have been attempted with limited success because of thickness limitations, deposition parameters which adversely affected fatigue life, corrosion resistance reduction due to galvanic action between coating and substrate, or application cost. Sputtering (Reference 84) offers one method for application which does not adversely affect the substrate; silicon carbide and tungsten carbide sputtered coatings have demonstrated some promise.

Titanium diboride (Reference 67) has exhibited excellent resistance to solid particle impact although it has not been optimized for jet engine applications.

2. CERAMICS

Impact erosion of ceramic materials has concentrated on rain erosion effects on tactical missile radome materials at high velocities until recently when solid particle erosion on refractory liners, runway debris on optical missile domes, and the desire to use ceramics in turbine engines to increase performance has led to consideration of such effects.

A summary of recent efforts to understand mechanisms of solid particle impact and analytically model those effects may be found in Reference 35.

As discussed in Section V, the use of ceramics with resistance to liquid impact has been limited because additional requirements for thermal shock resistance, fabricability, and lower cost have dictated the use of slip cast fused silica and pyroceram for missile radomes.

Recent research and development has explored reaction sintered and hot pressed silicon nitride for such applications, but the apparent sensitivity of these materials to surface flaw distribution has rendered their utility somewhat suspect. Fiber reinforced ceramic constructions such as silica with colloidal silica matrix, silica with ethyl silicate matrix, and alumina fabric with alumina matrix have also been evaluated but severe surface erosion was experienced even though catastrophic fracture did not occur (Reference 60).

Thin ceramic coatings have been utilized for composite radome construction protection with limited success (Reference 19). The key to utilization was maximizing the forgiveability of the coating to the impact so that it did not spall or fracture off due to coating-substrate impedance mismatch. A slip cast alumina shell adhesively bonded to glass-polyimide laminate withstood a Mach 3 multiple rain exposure while optimized plasma-sprayed coatings did not survive the test. Surface erosion was observed on the slip cast alumina but it did survive.

Solid particle erosion resistance of numerous refractory materials, ceramics, and cermets has been determined by Hansen (Reference 67). Materials such as boron carbide, tungsten carbide, silicon carbide, silicon nitride, and titanium diboride were found to have more than four times the erosion resistance of metals such as Stellite 6B and 304 and 316 stainless steel. Cubic boron nitride and industrial diamonds were found to not erode at all.

The use of ceramics for many large scale applications is of course dictated by economies of manufacture, installation, and maintenance. Discussion of these implications can be found in Reference 20.

3. ELASTOMERS

One of the most effective ways of combatting liquid impact erosion effects on reinforced plastic composites in aircraft has been the use of elastomeric coatings of thicknesses 0.2 mm to 0.3 mm (0.008 to 0.012 inches) (References 19, 77). These materials have been developed for aircraft radome protection to have combinations of rain erosion resistance, antistatic properties for reduction of precipitation static buildup on plastic surfaces, dielectric transmission for radar and other electromagnetic radiation, thermal flash resistance for protection from thermonuclear burst thermal pulse and room temperature curing, and spray application characteristics.

Coatings based upon neoprene rubber, which were developed in the early 1950's, have been superseded as the state-of-the-art by moisture curing and two component polyurethane coatings. The polyurethane coatings have proven to have greater erosion resistance, improved weathering characteristics, and much longer life in service than the neoprenes.

In addition, a class of coatings based upon fluorocarbon elastomers has also been developed which possesses long-term high temperature (260°C) capability and extremely good weatherability while maintaining the combinations of properties previously mentioned.

Solid particle erosion tests of these polyurethane and fluorocarbon coatings have demonstrated limited capability; however, the fluorocarbon coatings have shown sand erosion resistance at temperatures of 500°F in short duration exposures.

Tests on other elastomeric materials such as silicones have demonstrated no liquid impact erosion resistance due to the lack of tear resistance and inability to withstand the repeated deformations under drop impingement. By contrast, the polyurethane and fluorocarbon elastomeric coatings have high elongation, low modulus and moderate tensile strengths, and withstand impact for protracted periods.

The development of these coatings has been empirically based because the rotating arm simulation apparatus on which they have been tested provides a very close simulation of the subsonic rain impact conditions to which they are exposed and correlations have been developed between the modes of failure and relative rankings of materials in this apparatus and the actual performance in flight exposures.

4. PLASTICS

The erosion resistance of monolithic and reinforced plastics has been determined as a baseline substrate material which must be protected from liquid and solid impact. Only in a few isolated instances, i.e., protective covers for certain electromagnetic antennas, have these plastics been considered as erosion protective materials themselves (Reference 14).

Thermoplastic polymers such as nylon, acetal, polyethylene, and polyphenylene oxide have provided resistance to rain drop impact; although their application has been limited because of thermal and strength inadequacies.

Tests of reinforced composites have shown that chopped fiber reinforcement provides less erosion resistance than cloth reinforcement and that only by resorting to unusual construction, such as all fibers oriented end-on to the surface being impacted, could any significant erosion resistance be achieved. These unusual constructions are typically impractical because of lack of structural properties.

SECTION VII

DESIGN TECHNIQUES TO AVOID EROSION

The design methodology for avoiding erosion in impact situations is not well developed because, with the exception of some aerospace systems or components, erosion has typically been an after-the-fact occurrence or other requirements have dictated the configuration, choice of materials, or constraints on erosion prevention measures.

1. REDUCTION IN VELOCITY

As previously discussed, the velocity of impact is the most important variable in governing the severity of erosion and the most important influence on erosion rate. However, increased velocity is almost always desired whether it is aircraft and missile flight capability, turbine engine fan speed for efficiency, movement of coal particles in energy conversion processes or velocity of steam turbine generator blades.

Redesign of equipment to reduce the speed at which impacting drops or particles strike eroding surfaces should be accomplished whenever possible to reduce the velocity below the erosion threshold velocity.

2. REDUCTION IN IMPACT ANGLE

The variation of erosion rate in liquid impact depends upon the sine squared of the angle for composite laminates (Reference 52) and the sine cubed of the angle for 3-dimensionally reinforced carbon composites (Reference 2). Since most of the erosion processes are governed by the pressure loading as developed from the normal component of the velocity vector ($V \sin \theta$), reduction in the impact angle is perhaps the most effective design method for mitigating erosion effects in liquid impact.

The erosion rate varies with the angle for solid particle impact with ductile materials showing a maximum rate at 20-30 degrees and brittle materials showing a maximum for 90-degree impact. Therefore, depending upon the types of materials being protected, an impact angle selection and design must be based accordingly.

Angles of 15 degrees or less will usually minimize erosion.

3. REDUCTION IN DROPLET SIZE OR PARTICLE DIAMETER

The influence of droplet or particle size on erosion is a minor but important one. The smaller the drops or solid particles are, the less damage will be experienced.

One technique which is most appropriate is utilization of shock layer shattering and breaking up of rain drops to mitigate the impact damage by fragmenting the drops into very small pieces which do not damage aft surfaces at supersonic speeds. This phenomenon has been the subject of numerous papers and sessions at international erosion conferences and the knowledge on the subject is summarized in References 85 and 86.

The shock layer protection has been extended to optical domes and even to certain cone shapes by use of tapered cylindrical covers over the optical domes or wide annular rings at the base of the cones. The shock layer attached to these fixtures provides sufficient distance from the shock to the surface to enable shattering to occur. Obviously these techniques apply primarily to liquid impact supersonically, as the shock layer will have no effect on solid particles and even deflection will be minimized (References 87, 88).

4. PARTICLE CONCENTRATION REDUCTION

Since the erosion is directly proportional to the number of particles being struck, the elimination or reduction of significant numbers of particles is desired for protection of surfaces and components.

Liquid impact has caused speculation for debris layer shielding of materials due to impacted water layer and/or target debris on the surface. This would reduce erosion since that layer would absorb considerable energy of impact and reduce the loads delivered to the material surface. However, some evidence exists for little or no effects of this layer (Reference 89) and others for some measurable shielding provided by this layer.

Solid particle centrifugal separators have been used on helicopter engines for reducing the concentration of particles ingested into the inlet. Although these separators result in performance penalties, they are successful in prolonging the life of engine blades operating in dusty environments. Similar techniques may likely be required for direct gasification in coal energy systems.

5. LEADING EDGE RADIUS EFFECTS

The sharpness of the leading edge in turbine blades, aircraft airfoils, or other forward facing surfaces has an interesting effect on liquid impact erosion. Although no quantitative studies have been done, many investigators have observed that erosion is aggravated when the leading edge radius is reduced so that the dimensions of the edge are similar to or less than the impacting drops. The concentration of stresses under the impact loading aggravates damage while in a blunter shape, these stresses are dissipated with correspondingly less damage.

The only method known to reduce these effects is to make saw teeth in the knife edge. Experiments at the Air Force Materials Laboratory on composite knife edge specimens showed that sizing of the tooth point-to-point spacing versus depth could be optimized to cause significant reduction in erosion (Reference 90). No such effects of leading edge radius are known in solid particle erosion.

6. FLUSH MOUNTING/GRADUAL BENDS

The impact of liquid drops on surfaces shows that preferential attack will occur at any discontinuity in the surface, even though the two sides of the seam are flush mounted. This occurs in high speed liquid impact but has also been observed in low speed rotating arm tests.

The design of radomes with very slender ogival or conical shapes (for drag purposes) has typically employed a sharp pointed metal cone for erosion protection in the 90-degree impact area. However, it has been essential to include a conical base diameter of the metal which slightly extends beyond the outer radius of the ceramic tip to prevent

attack of the ceramic at that edge with fracture and potential loss of the tip.

Flush mounting is desired since major discontinuities will be immediately attacked. However, any holes (for example, the back edge of a Phillips head slot in a bolt) which are oriented perpendicular to the flowing drop can be attacked.

Similar results have been experienced for misaligned pipe carrying flowing solid particles either entrained in a gas or in a liquid slurry. The preferential attack has caused failures as the edges are eroded and widened. Extremely careful alignment and minimization of discrepancies at weld joints are the guidelines to be followed.

Another aspect of this problem is the desirability of large radius bends in pipe or ducting carrying solid particles to avoid erosion at elbows. Since the impact velocity of the particles against the surface governs the erosion, reduction of that velocity by a gradual curvature which minimizes normal impact can provide change in particle direction without the serious erosion otherwise experienced.

Another technique is a dead tee where the particles build up in the blocked end of a tee and then conform to flow streamlines so that particles changing directions impact other particles rather than the walls of the tube or pipe.

7. GEOMETRY AND SCALE-UP

The methodology for assessing full size geometry and scale-up effects for erosion has not been developed. Typically, small simple specimen shapes are used for erosion testing and estimates are then made of effects to be anticipated on a large scale.

AFML-TR-79-4122

In the case of ceramics for tactical missile radomes, the proof of the erosion resistance of a particular material can only be proven by fabrication of a piece of prototype hardware which has realistic attachment fixtures and testing it in a simulated rain environment (such as a prototype radome propelled through the rainfield on a rocket sled at Holloman AFB).

Similar considerations apply to ceramics for large scale equipment in coal conversion plants, metals in combined corrosive erosive environments, and numerous other situations. Attempts to describe and predict effects in large scale equipment are becoming more available in literature (References 20, 53).

SECTION VIII

CONCLUSIONS

The science of liquid and solid impact erosion is growing rapidly. The vast quantities of empirical and screening data which have provided rankings of performance of materials and the basis for selection of erosion resistant materials are now being supplemented with analytical models and mechanistic understanding for improved analysis of erosion processes.

The guidelines for improved erosion resistance in materials which have been obtained through experimental testing have been successful in developing better materials. However, the methodology for predicting in-service performance and the lifetime of materials in erosive environments is still in its infancy. Careful review of past experience with materials approaches, design techniques, and practical protective methods can enable selection and design of erosion resistant components and structures.

REFERENCES

1. W. F. Adler, "The Mechanics of Liquid Impact", Treatise on Materials Science and Technology, Vol. 16, Academic Press, 1978.
2. G. F. Schmitt, "Influence of Materials Construction Variables on the Rain Erosion Performance of Carbon-Carbon Composites," Erosion; Prevention and Useful Applications, ASTM-STP-664, W. F. Adler, ed., American Society for Testing and Materials, 1979, pp. 375-405.
3. W. F. Adler and S. V. Hooker, "Rain Erosion Mechanisms in Brittle Materials," Wear, 50 1978, pp 11-38.
4. T. L. Peterson, "Multiple Water Drop Impact Damage in Layered Infrared Transparent Materials", Erosion; Prevention and Useful Applications, ASTM-STP-664, W. F. Adler Ed., American Society for Testing and Materials, 1979, pp. 279-297.
5. D. J. Beckwith and J. B. Marriott, "Water Jet Impact Damage in a Cobalt-Chromium-Tungsten Alloy", Erosion by Cavitation or Impingement, ASTM-STP-408, American Society for Testing and Materials, 1967, pp. 111-124.
6. F. J. Heymann, "A Survey of Clues to the Relationship between Erosion Rate and Impact Parameters", Proceedings of the Second Meersburg Conference on Rain Erosion and Allied Phenomena, A. A. Fyall and R. B. King, Eds., Royal Aircraft Establishment, Farnborough, England, 1967, pp. 264.
7. G. S. Springer, Erosion by Liquid Impact, Scripta Publishing Company, John Wiley & Sons, Washington, DC, 1976, pp. 264.
8. W. F. Adler and R. F. Vyhna1, "Rain Erosion of Ti-6Al-4V," Proceedings of the Fourth International Conference on Rain Erosion and Associated Phenomena, A. A. Fyall and R. B. King, Eds., Royal Aircraft Establishment, Farnborough, England, 1974, pp. 539-569.
9. H. Rieger, "The Damage to Metals on High Speed Impact with Water Drops," Proceedings of the Rain Erosion Conference Held at Meersburg, West, Germany, A. A. Fyall and R. B. King, Eds., Royal Aircraft Establishment, Farnborough, England, 1965, pp. 107-113.
10. "Standard Terminology Relating to Erosion and Wear, ASTM Standard G40-77, American Society for Testing and Materials 1978 Annual Book of Standards, Philadelphia, PA Part 10, pp. 827-833.
11. A. Thiruvengadam, "The Concept of Erosion Strength," Erosion by Cavitation or Impingement, ASTM-STP-408, American Society for Testing and Materials, 1967, pp. 22-35.
12. W. F. Adler and S. V. Hooker, Characterization of Transparent Materials for Erosion Resistance, AFML-TR-76-16, Air Force Materials Laboratory, Wright-Patterson Air Force Base, Ohio, 1976.

REFERENCES (Cont'd)

13. G. F. Schmitt, "The Erosion Behavior of Polymeric Coatings and Composites at Subsonic Velocities," Proceedings of Third International Conference on Rain Erosion and Associated Phenomena, A. A. Fyall and R. B. King, Eds., Royal Aircraft Establishment, Farnborough, England, 1970, pp. 107-128.
14. G. F. Schmitt, "Materials Parameters that Govern the Erosion Behavior of Polymeric Composites in Rain Environments," Composite Materials: Testing and Design (Third Conference), ASTM-STP-546, American Society for Testing and Materials, 1974, pp. 303-323.
15. D. A. Gorham, M. J. Matthewson, and J. E. Field, "Damage Mechanisms in Polymers and Composites Under High-Velocity Liquid Impact," Erosion: Prevention and Useful Applications, ASTM-STP-664, American Society for Testing and Materials, 1979, pp. 320-342.
16. G. F. Schmitt, "Polyurethane Coatings for Rain Erosion Protection," Proceedings of the Second Meersburg Conference on Rain Erosion and Allied Phenomena, A. A. Fyall and R. B. King, Eds., Royal Aircraft Establishment, Farnborough, England, 1967, pp. 329-357.
17. H. Rieger and H. Boche, "Erosion Behavior of Surface Coatings," Proceedings of the Fourth International Conference on Rain Erosion and Associated Phenomena, A. A. Fyall and R. B. King, Eds., Royal Aircraft Establishment, Farnborough, England, 1974, pp. 637-675.
18. G. F. Schmitt, "Elevated Temperature Resistant, Subsonic Rain Erosion Resistant Fluoroelastomer Radome Coatings," Proceedings of the Third International Conference on Electromagnetic Windows, Paris, France, 1975, pp. 211-232.
19. G. F. Schmitt, "Advanced Rain Erosion Resistant Coating Materials," Science of Advanced Materials and Process Engineering Series, Vol. 18, 1973, pp. 57-75.
20. Erosion Control in Energy Systems, NMAB-334, National Materials Advisory Board, National Academy of Science, Nov. 1977, pp. 228.
21. L. K. Ives and A. W. Ruff, "Electron Microscopy Study of Erosion Damage in Copper," Erosion: Prevention and Useful Applications, ASTM STP-664, W. F. Adler, Ed., American Society for Testing and Materials, 1979, pp. 5-35.
22. I. Finnie, A. Levy, and D. H. McFadden, "Fundamental Mechanisms of the Erosive Wear of Ductile Metals by Solid Particles," Erosion: Prevention and Useful Applications, ASTM-STP-664, W. F. Adler, Ed., American Society for Testing and Materials, 1979, pp. 36-58.
23. I. Hutchings, "Mechanisms of the Erosion of Metals by Solid Particles," Ibid, pp 59-76.

REFERENCES (Cont'd)

24. J. Maji and G. L. Sheldon, "Mechanisms of Erosion of a Ductile Material by Solid Particles," Ibid, pp. 136-147.
25. J. G. A. Bitter, Wear, Vol. 6, 1963, pp. 5-21 and pp. 169-190.
26. G. P. Tilly, Wear, Vol. 14, 1969, pp. 63-79 and pp. 241-248; Vol. 16, 1970, pp 447-465 and Vol. 23, 1973, pp. 87-96.
27. C. E. Smeltzer, M. E. Gulden, and W. A. Compton, Transactions of ASME, Vol. 92, 1970, pp. 639-654.
28. G. L. Sheldon and A. Kanhere, Wear, Vol. 21, 1972, pp. 195-209.
29. P. Ascarelli, Relations Between the Erosion by Solid Particles and the Physical Properties of Metals, AMMRC-TR-71-47, Army Materials and Mechanics Research Center, Watertown, MA, 1971.
30. W. F. Adler, Analysis of Multiple Particle Impacts on Brittle Materials, AFML-TR-74-170, Air Force Materials Laboratory, Wright-Patterson Air Force Base, Ohio, 1974.
31. P. A. Engle, Impact Wear of Materials, Elsevier Scientific Publishing Company, Amsterdam, 1976, pp. 333 (See Chapters 4 and 5).
32. A. G. Evans, M. E. Gulden, G. E. Eggum, and M. Rosenblatt, Impact Damage in Brittle Materials in the Plastic Response Regime, Contract No. 00014-75-C-0069, Report No. SC5023.9TR, Rockwell International Science Center, Thousand Oaks, CA, 1976.
33. M. E. Gulden, "Solid Particle Erosion of High Technology Ceramics (Si_3N_4 , Glass-Bonded Al_2O_3 , and MgF_2)," Erosion: Prevention and Useful Applications, ASTM-STP-664, W. F. Adler, Ed., American Society for Testing and Materials, 1979, pp. 101-122.
34. A. G. Evans and T. R. Wilshaw, "Dynamic Solid Particle Damage in Brittle Materials: An Appraisal," J. Materials Science, 12, 1977, p. 97.
35. A. W. Ruff and S. M. Wiederhorn, Erosion by Solid Particle Impact, NBSIR 78-1575. National Bureau of Standards Interim Report, January 1979, AD No. A066-525.
36. A. Thiruvengadam, "Theory of Erosion," Proceedings of Second Meersburg Conference on Rain Erosion and Allied Phenomena, A. A. Fyall, and R. B. King, Eds., Royal Aircraft Establishment, Farnborough, England, 1967, pp. 605-649.
37. G. S. Springer and C. B. Baxi, "A Model for Rain Erosion of Homogeneous Materials," Erosion, Wear and Interfaces with Corrosion, ASTM-STP-567, American Society for Testing and Materials, 1974, pp. 106-127.

REFERENCES (Cont'd)

38. G. S. Springer and C. I. Yang, "A Model for the Rain Erosion of Fiber Reinforced Composites," AIAA Journal, 13, 1975, pp. 887-883.
39. G. S. Springer, C. I. Yang, and P. S. Larsen, "Rain Erosion of Coated Composites," Journal of Composite Materials, 8, 1974, pp. 229-250.
40. G. S. Springer and C. I. Yang, "Optical Transmission Losses of Materials due to Repeated Impacts of Liquid Droplets," AIAA Journal, 1975, pp. 1483-1487.
41. W. F. Adler, Wear, 37, 1976; pp. 345-352.
42. O. G. Engel, A Model for Multiple Drop Impact Erosion of Brittle Materials, General Electric Report GESP-610, 1971.
43. H. Hertz, Miscellaneous Papers, MacMillan and Company, London, 1886.
44. O. G. Engel, Mechanisms of Rain Erosion Part I. Impact Pressure in Solid-Liquid Sphere Collisions, WADC-TR-53-192, Part I, Wright Air Development Center, Wright-Patterson Air Force Base, Ohio, 1953.
45. O. G. Engel, J. Research NBS, 64A, 1960, pp. 497-498.
46. F. J. Heymann, Erosion by Cavitation, Liquid Impingement and Solid Impingement - A Review, Westinghouse Electric Corp. Eng Report E-1460, 1968.
47. Y. Huang, Numerical Studies of Unsteady Two Dimensional Liquid Impact Phenomena, PHD Thesis, University of Michigan, Ann Arbor, 1971.
48. J. B. Hwang, The Impact Between a Liquid Drop and an Elastic Half Space, PHD Thesis, University of Michigan, Ann Arbor, 1975.
49. M. Rosenblatt, L. A. DeAngelo, F. E. Eggum, and K. N. Krevenhagen, Numerical Investigations of Water Drop Erosion Mechanisms in Infrared Transparent Materials, AFML-TR-76-193, Air Force Materials Laboratory, Wright-Patterson Air Force Base, Ohio, 1976.
50. M. C. Rochester and J. H. Brunton, "Surface Pressure Distribution During Drop Impingement," Proceedings of the Fourth International Conference on Rain Erosion and Associated Phenomena, A. A. Fyall and R. B. King, Eds., Royal Aircraft Establishment, Farnborough, England, 1974, pp. 371-393.
51. W. Johnson and G. W. Vickers, J. Mechanical Engineering Science, 15, 1973, pp. 302-310.
52. G. F. Schmitt, "Erosion Rate-Velocity Dependence for Materials at Supersonic Speeds," Characterization and Determination of Erosion Resistance, ASTM-STP-474, American Society for Testing and Materials, 1970, pp. 323-352.

REFERENCES (Cont'd)

53. M. Mengeturk and E. F. Sverdrup "Calculated Tolerance of a Large Electric Utility Gas Turbine to Erosion Damage by Coal Gas Ash Particles," Erosion: Prevention and Useful Applications, ASTM-STP-664, W. F. Adler, Ed., American Society for Testing and Materials, 1979, pp. 193-224.
54. G. Hoff, G. Langbein, and H. Rieger, "Material Destruction due to Liquid Impact," Erosion by Cavitation or Impingement, ASTM-STP-408, American Society for Testing and Materials, 1967, pp. 42-69.
55. A. Thiruvengadam and S. L. Rudy, Experimental and Analytical Investigations of Multiple Liquid Impact Erosion, Technical Report 719/1, NASA Contract NASW-1608, June 1968.
56. L. B. Weckesser, "An Approximate Procedure for Defining Pyroceram 9606 Failure in Rain," Proceedings of the Thirteenth Symposium on Electromagnetic Windows, Georgia Institute of Technology, Atlanta, Ga., 1976, pp. 65-66.
57. G. F. Schmitt and C. J. Hurley, Development and Calibration of a Mach 1.2 Rain Erosion Test Apparatus, AFML-TR-70-240, Air Force Materials Laboratory, Wright-Patterson AFB, Ohio, 1970.
58. G. F. Schmitt, "Rain Droplet Erosion Effects on Transparent Plastic Materials," SAMPE Journal, Vol. 10, No. 2, March/April 1974, pp. 16-24.
59. G. F. Schmitt, "Erosion Behavior of Materials in Rain at High Velocities," High Temperatures-High Pressures, Vol. 6, 1974, pp. 177-188.
60. G. F. Schmitt, "Influence of Antenna Window Materials Construction Parameters on Erosion Behavior at Hypersonic Velocities," Proceedings of the Twelfth Symposium on Electromagnetic Windows, Georgia Institute of Technology, Atlanta, GA, 1974, pp. 121-127.
61. Basic Investigation of Turbine Erosion Phenomena, Westinghouse Astronuclear Laboratory, Report WANL-TME-1977, Revision I, NASA Contract NAS 7-390, January 1971.
62. D. W. C. Baker, D. E. Elliott, D. G. Jones, and D. Pearson, "The Erosion Resistance of Steam Turbine Blade and Shield Materials," Proceedings of the Second Meersburg Conference on Rain Erosion and Allied Phenomena, A. A. Fyall and R. B. King, Eds., Royal Aircraft Establishment, Farnborough, England, 1967, pp. 449-513.
63. D. E. Elliott, J. B. Mariotti, and A. Smith, "Comparison of Erosion Resistance of Standard Steam Turbine Blade and Shield Materials on Four Test Rigs," Characterization and Determination of Erosion Resistance, ASTM-STP-474, American Society for Testing and Materials, 1970, pp. 127-161.

REFERENCES (Cont'd)

64. J. V. Hackworth, L. H. Kocher, and I. C. Snell, "Response of Infrared Transmitting Materials to High Velocity Impact by Water Drops," Erosion: Prevention and Useful Applications, ASTM-STP-664, W. F. Adler, Ed., American Society for Testing and Materials, 1979, pp. 255-278.
65. G. Hoff, "Rain Erosion of Glass and Ceramics," Proceedings of the Rain Erosion Conference Held at Meersburg, West Germany, A. A. Fyall and R. B. King, Eds., Royal Aircraft Establishment, Farnborough, England, 1965, pp 90-94.
66. G. Hoff and H. Rieger, "Rain Erosion of Infrared Transmitting Materials," Proceedings of the Eleventh Symposium on Electromagnetic Windows, Georgia Institute of Technology, Atlanta, GA, 1972, pp. 93-97.
67. J. S. Hansen, "Relative Erosion Resistance of Several Materials," Erosion: Prevention and Useful Applications, ASTM-STP-664, W. F. Adler, Ed. American Society for Testing and Materials, 1979, pp. 148-162.
68. C. E. Smeltzer, M. E. Gulden, S. S. McElmury, and W. A. Compton, Mechanisms of Sand and Dust Erosion in Gas Turbine Engines, US Army Aviation Material Laboratories Technical Report 70-36, Fort Eustis, VA, 1970.
69. G. P. Tilly and W. Sage, National Gas Turbine Establishment, ASME Paper No. 69-WA/Met-6, Winter Annual Meeting, Los Angeles, CA, Nov. 1969.
70. G. T. Sheldon, Similarities and Differences in the Erosion Behavior of Materials, ASME Paper No. 69-WA/Met-7, Winter Annual Meeting, Los Angeles, CA, Nov. 1969.
71. G. Grant and W. Tabakoff, "Erosion Prediction in Turbomachinery Resulting from Environmental Solid Particles," Journal of Aircraft, Vol. 12, No. 5, May 1975, pp. 471-478.
72. W. Tabakoff and T. Wakeman, "Test Facility for Material Erosion at High Temperature," Erosion: Prevention and Useful Applications, ASTM-STP-664, W. F. Adler, Ed., American Society for Testing and Materials, 1979, pp. 123-135.
73. G. C. Gould, "Some Observations on Erosion by Cavitation and Impingement," Characterization and Determination of Erosion Resistance ASTM-STP-474, American Society for Testing and Materials, 1970, pp. 182-211.
74. A. Thiruvengadam, S. L. Rudy, and M. Gunasekaran, "Experimental and Analytical Investigations on Liquid Impact Erosion," Characterization and Determination of Erosion Resistance, ASTM-STP-474, American Society for Testing and Materials, 1970, pp. 249-287.

REFERENCES (Cont'd)

75. J. M. Hobbs, "Experience with a 20 kc Cavitation Test," Erosion by Cavitation and Impingement, ASTM-STP-408, American Society for Testing and Materials, 1967, pp. 159-185.
76. G. C. Gould, "Cavitation Erosion of Stellite and Other Metallic Materials," Proceedings of the Third International Conference on Rain Erosion and Associated Phenomena, A. A. Fyall and R. B. King, Eds., Royal Aircraft Establishment, Farnborough, England, 1970, pp. 881-906.
77. G. F. Schmitt, Impact Erosion - A Serious Environmental Threat to Aircraft and Missiles, ASME Paper No. 75-ENAS-45, Intersociety Conference on Environmental Systems, San Francisco, CA, July 1975.
78. G. F. Schmitt, "In Service Performance of Polyurethane and Fluorocarbon Rain Erosion Resistant Radome Coatings," Materials & Processes - In Service Performance, Science of Advanced Materials and Process Engineering Series, Vol. 9, 1977, pp. 377-391.
79. A. F. Conn and A. Thiruvengadam, "Dynamic Response and Adhesion Failures of Rain Erosion Resistant Coatings," Journal of Materials, JMLSA, Vol. 5 No. 3, Sept. 1970, pp. 698-718.
80. H. Oberst, Rain Erosion and Molecular Properties of Synthetic Materials, Royal Aircraft Establishment Library Translation No. 1335, Farnborough, England, Dec. 1968.
81. G. F. Schmitt, "Influence of Porosity and Density on the Supersonic Rain Erosion Behavior of Silicon Nitride Radome Materials," Proceedings of the Thirteenth Symposium on Electromagnetic Windows, Georgia Institute of Technology, Atlanta, GA, 1976, pp. 37-44.
82. G. F. Schmitt, "On the Dependence of Materials Erosion on Environmental Parameters at Supersonic Velocities," Journal of Aircraft, Vol. 10 No. 2, Dec 1973, pp. 706-709.
83. J. H. Weaver, "Electroplated Nickel Rain Erosion Resistant Coatings," Proceedings of the Second Meersburg Conference on Rain Erosion and Allied Phenomena, A. A. Fyall and R. B. King, Eds., Royal Aircraft Establishment, Farnborough, England, 1967, pp. 401-426.
84. K. Gentner, "Thin Erosion Resistant Coatings, Applied by Means of Sputtering Techniques," Proceedings of the Fourth International Conference on Rain Erosion and Associated Phenomena, A. A. Fyall and R. B. King, Eds., Royal Aircraft Establishment, Farnborough, England, 1974, pp. 701-714.
85. W. G. Reinecke, G. D. Waldman, and W. L. McKay, "A General Correlation of Flow-induced Drop Acceleration, Deformation and Shattering," Proceedings of the Fifth International Conference on Erosion by Liquid and Solid Impact, Cambridge, England, 3-6 September 1979.

REFERENCES (Cont'd)

86. W. G. Reinecke and G. D. Waldman, "Shock Layer Shattering of Cloud Drops in Reentry Flight," AIAA Paper 75-152, AIAA Thirteenth Aerospace Sciences Meeting, Pasadena, CA 1975.
87. R. H. Adams and M. R. Smith, "Design and Development of RECAP, an Aerodynamic Device for Rain Erosion Protection of Optical Domes on Missiles," Proceedings of the Third International Conference on Rain Erosion and Associated Phenomena, A. A. Fyall and R. B. King, Eds., Royal Aircraft Establishment, Farnborough, England, 1970, pp. 935-968.
88. R. B. King, "Protection of Missile Domes from Rain Erosion Damage by Means of Aerodynamic Breakup of Drops," Proceedings of Fourth International Conference on Rain Erosion and Associated Phenomena, A. A. Fyall and R. B. King, Eds., Royal Aircraft Establishment, Farnborough, England, 1974, pp. 63-95.
89. G. F. Schmitt, "Influence of Rainfall Intensity on Erosion of Materials at Supersonic Velocities," J. Aircraft, Vol. 12, No. 10, Oct. 1975, pp. 761-762.
90. G. F. Schmitt, Unpublished results.

BIBLIOGRAPHY

The following bibliography comprises major documents in the erosion area which should be consulted by anyone interested in becoming familiar with the erosion literature.

PERIODICAL

Wear magazine published monthly by Elsevier Sequoia, Lausanne, Switzerland

BOOKS

Peter A. Engel, Impact Wear of Materials, Elsevier Scientific Publishing Company, Amsterdam, 1976, pp. 339.

George S. Springer, Erosion by Liquid Impact, Scripta Publishing Co., John Wiley & Sons, New York, 1976, pp. 264.

C. M. Preece, Ed. Treatise on Materials Science and Technology, Vol. 16, Academic Press, New York, 1978.

Erosion: Prevention and Useful Applications, ASTM-STP-664, W. F. Adler, Editor, American Society for Testing and Materials, Philadelphia, 1979, pp. 643.

Erosion, Wear and Interfaces with Corrosion, ASTM-STP-567, 1974, pp. 335.

Characterization and Determination of Erosion Resistance, ASTM-STP-474, 1970, pp. 434.

Erosion by Cavitation or Impingement, ASTM-STP-408, 1967, pp. 283.

Symposium on Erosion and Cavitation, ASTM-STP-307, 1961, pp. 98.

CONFERENCE PROCEEDINGS

Proceedings of the Rain Erosion Conference Held at Meersburg, West Germany, A. A. Fyall and R. B. King, Editors, Royal Aircraft Establishment, Farnborough, England, 1965, pp. 214.

Proceedings of the Second Meersburg Conference on Rain Erosion and Allied Phenomena, A. A. Fyall and R. B. King, Editors, Royal Aircraft Establishment, Farnborough, England, 1967, pp. 826.

Proceedings of the Third International Conference on Rain Erosion and Associated Phenomena, A. A. Fyall and R. B. King, Editors, Royal Aircraft Establishment, Farnborough, England, 1974, pp. 925.

BIBLIOGRAPHY (Cont'd)

Proceedings of the Fourth International Conference on Rain Erosion and Associated Phenomena, A. A. Fyall and R. B. King Editors, Royal Aircraft Establishment, Farnborough, England, 1974, pp. 925.

Proceedings of the Fifth International Conference on Erosion by Liquid and Solid Impact, Cambridge, England, 3-6 September 1979, Royal Aircraft Establishment, Farnborough, England.

REPORTS

Erosion Control in Energy Systems, NMAB-334, National Materials Advisory Board, National Academy of Science, November 1977, pp. 228.

Erosion by Solid Particle Impact, NBSIR78-1575, National Bureau of Standards, Washington, DC., January 1979, pp. 104.

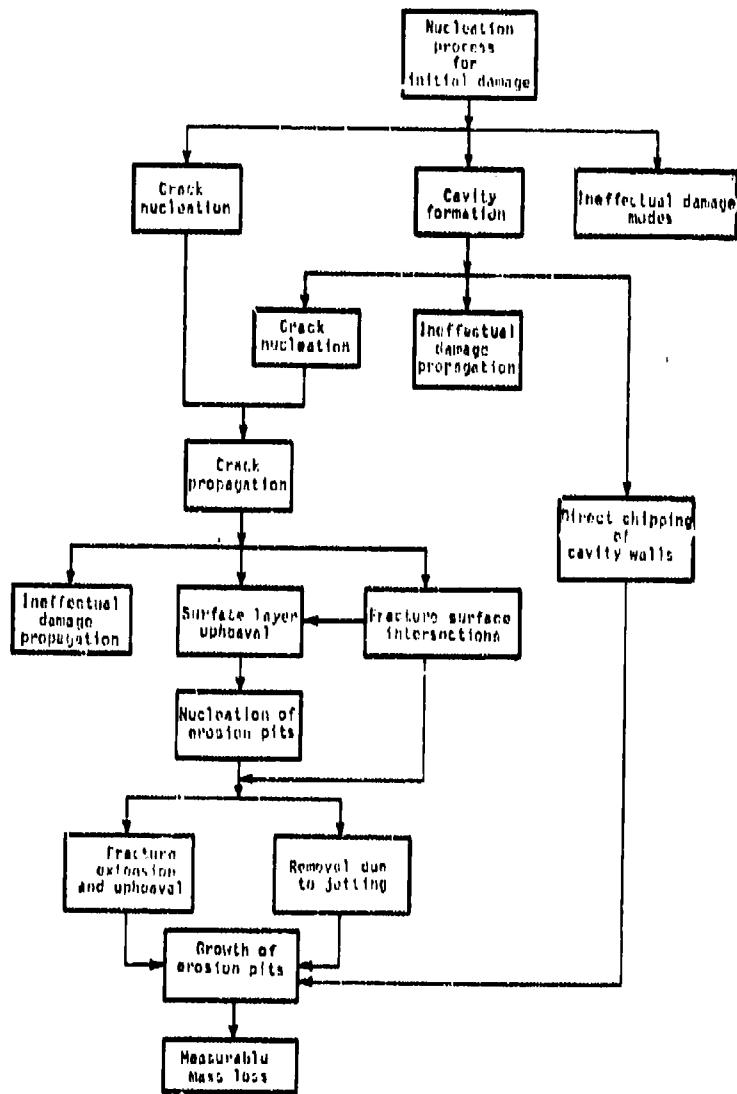


Figure 1. Damage Modes Due to Liquid Drop Impingement

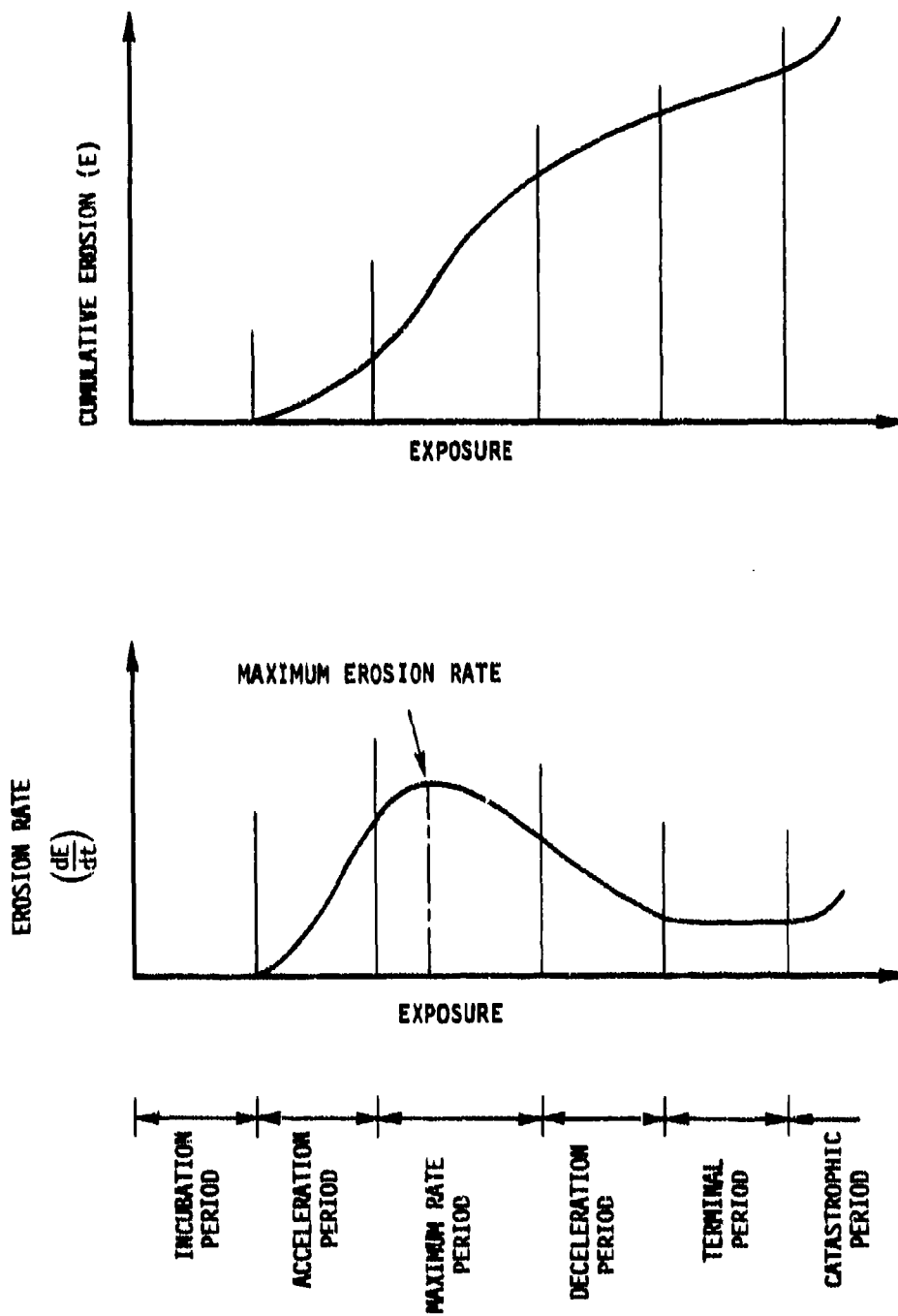


Figure 2. Erosion Rate/Cumulative Erosion

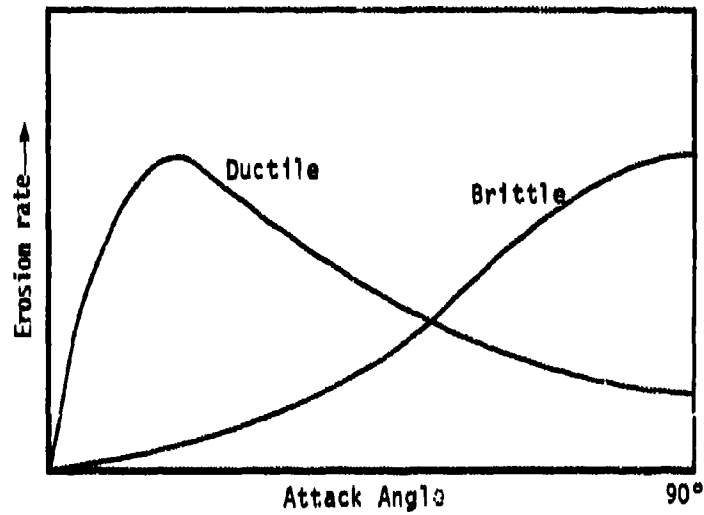


Figure 3. Dependence of Erosion Rate on Attack Angle is Shown Schematically for Ductile and Brittle Materials

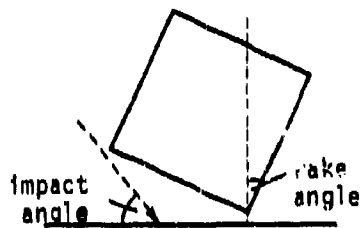


Figure 4. Impact of Rectangular Plate Showing Definitions of Impact Angle and Rake Angle

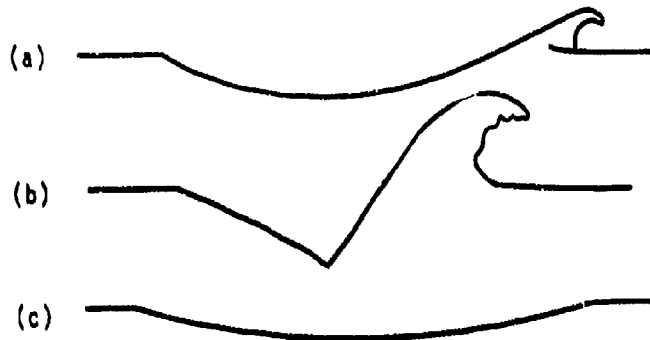


Figure 5. Sections Through Impact Craters Showing Typical Shapes

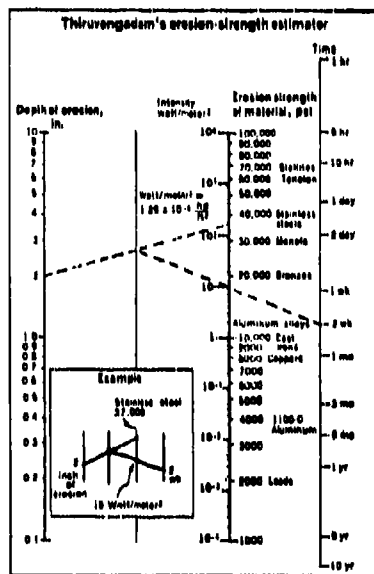


Figure 6. Thiruvengadam's Erosion Strength Estimator

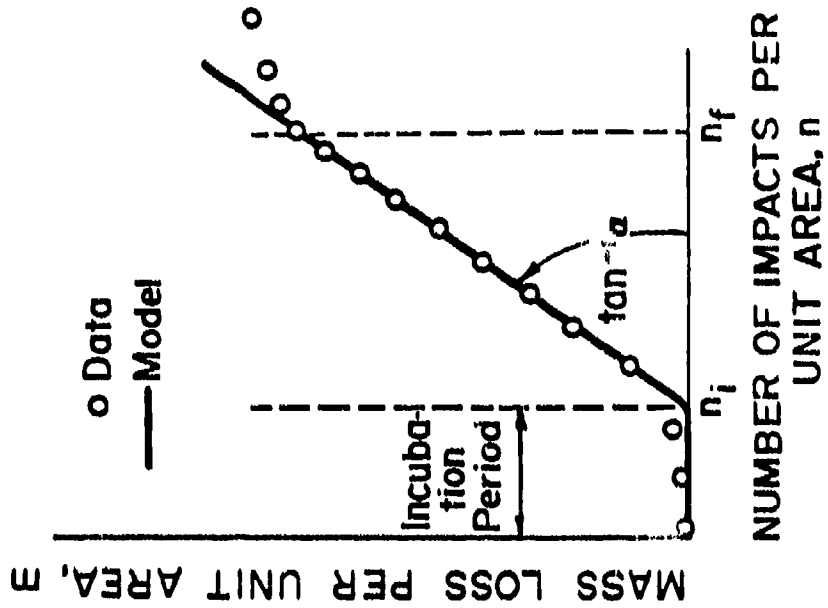


Figure 7a. Schematic of the Experimental Results

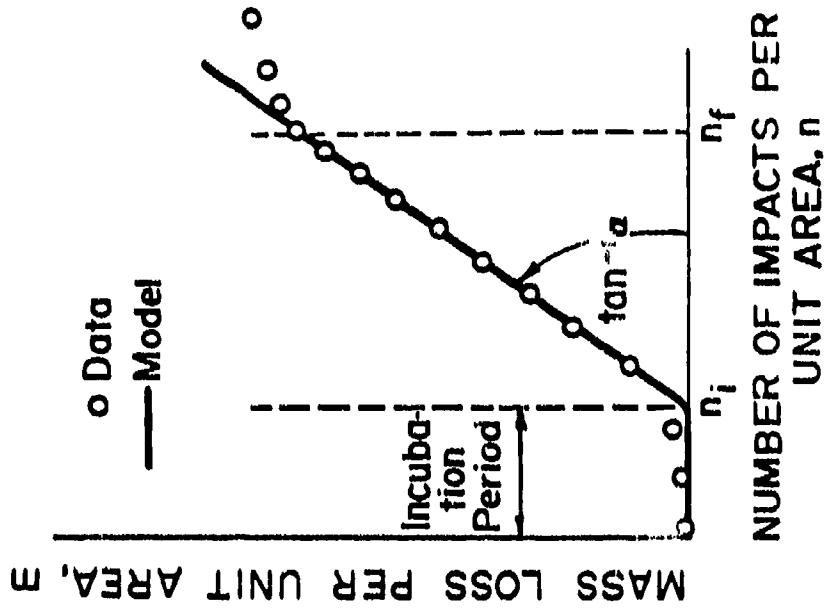


Figure 7b. The Solution Model

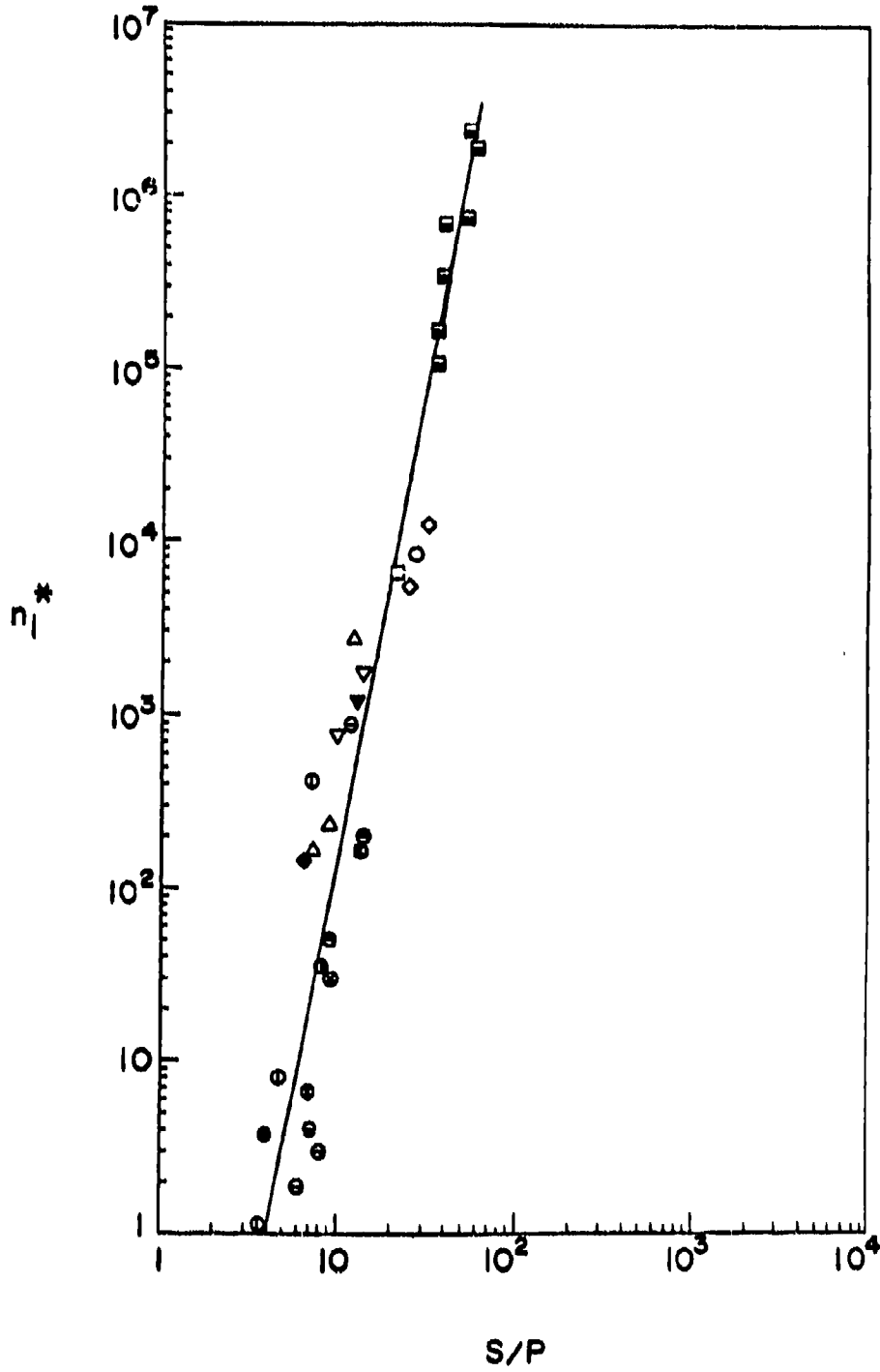


Figure 8. Incubation Period Versus S/P

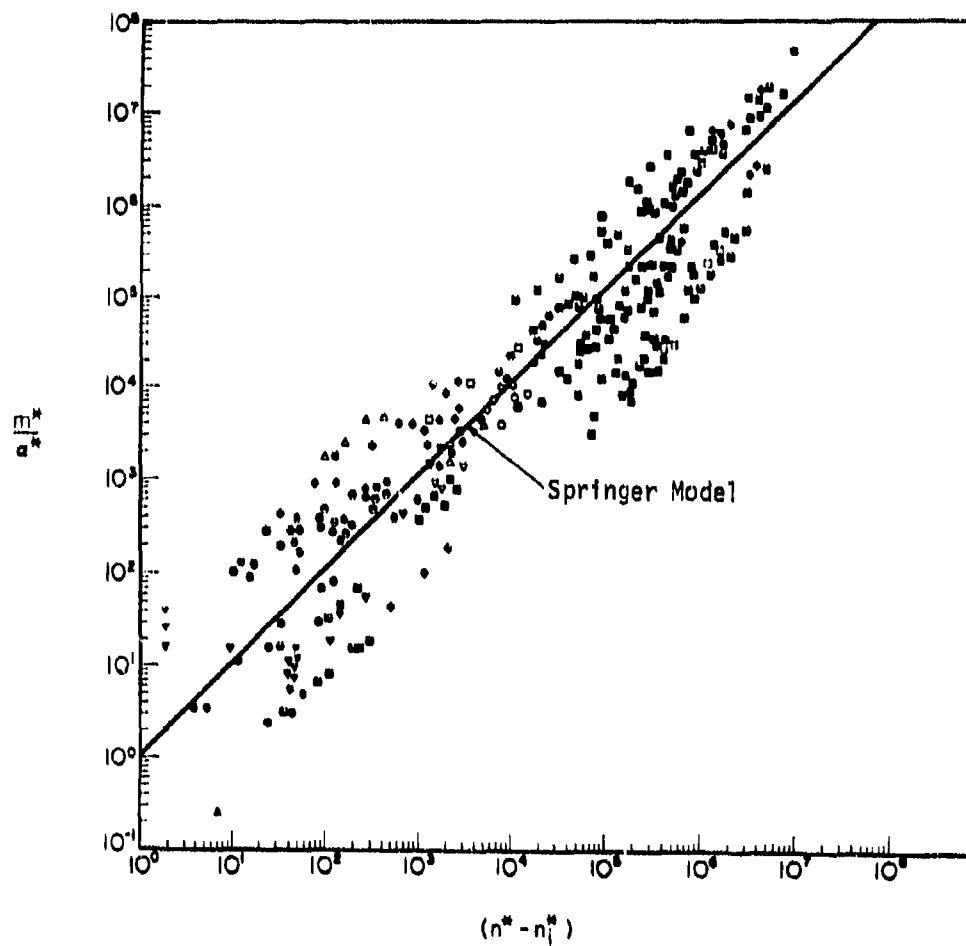


Figure 9. Comparison of Springer Model with Experimental Results

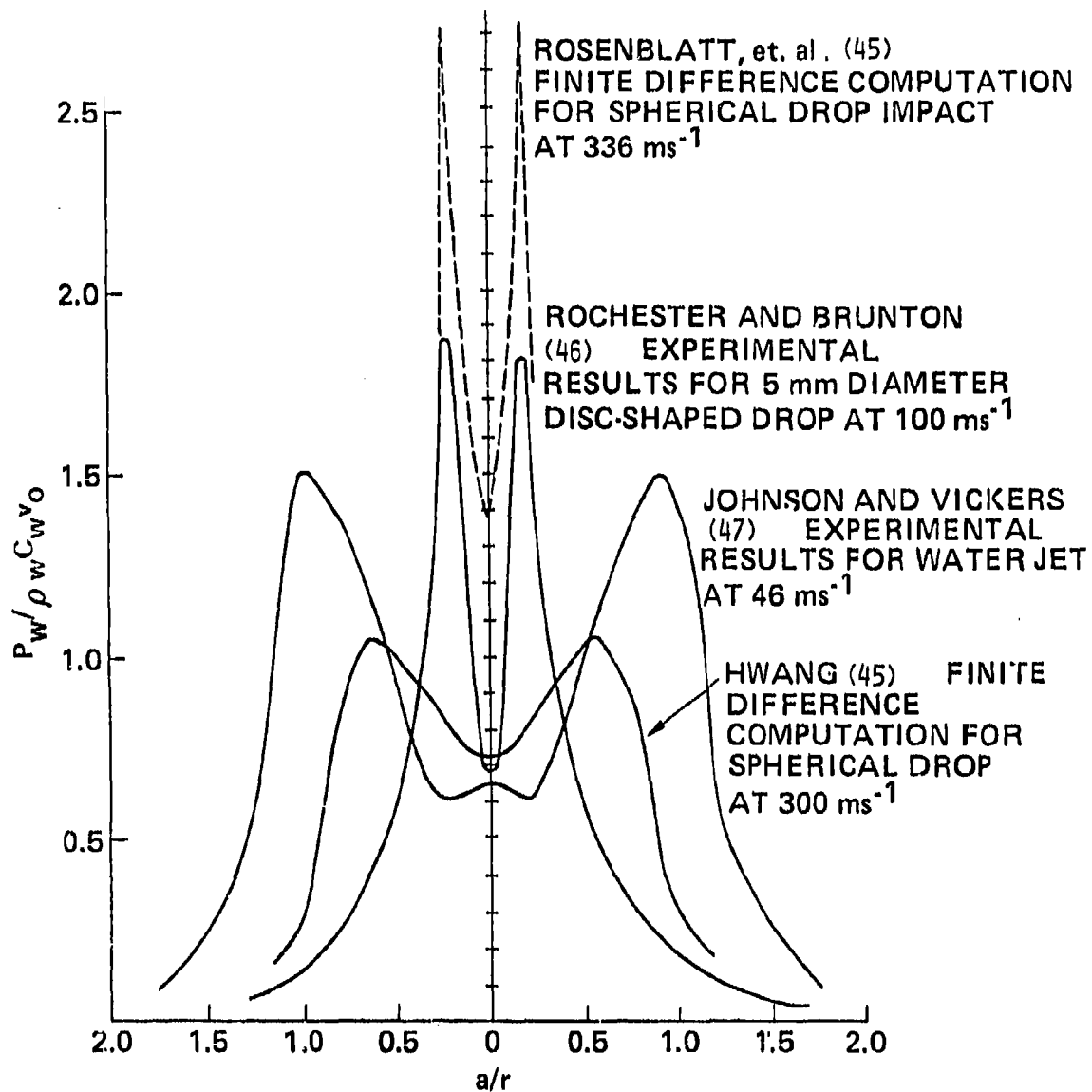


Figure 10. Pressure Distribution Under Impacting Water Drop

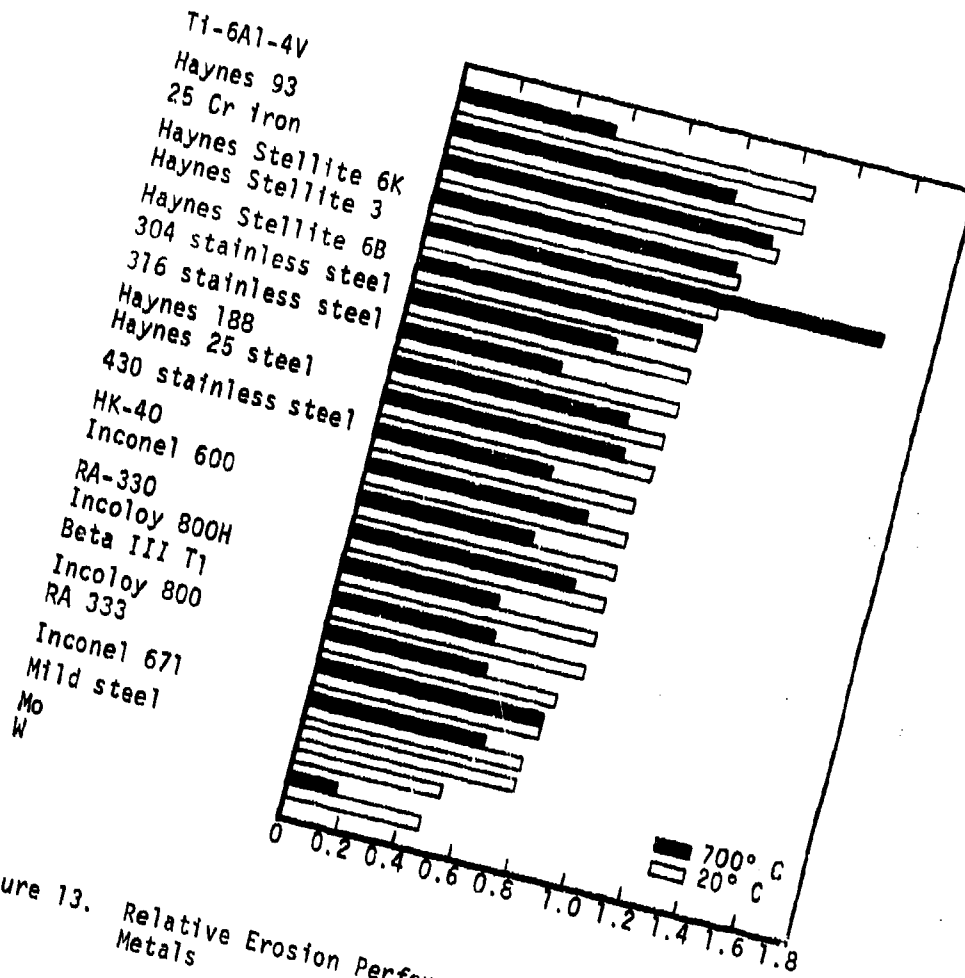


Figure 13. Relative Erosion Performance of Commercially Available Metals

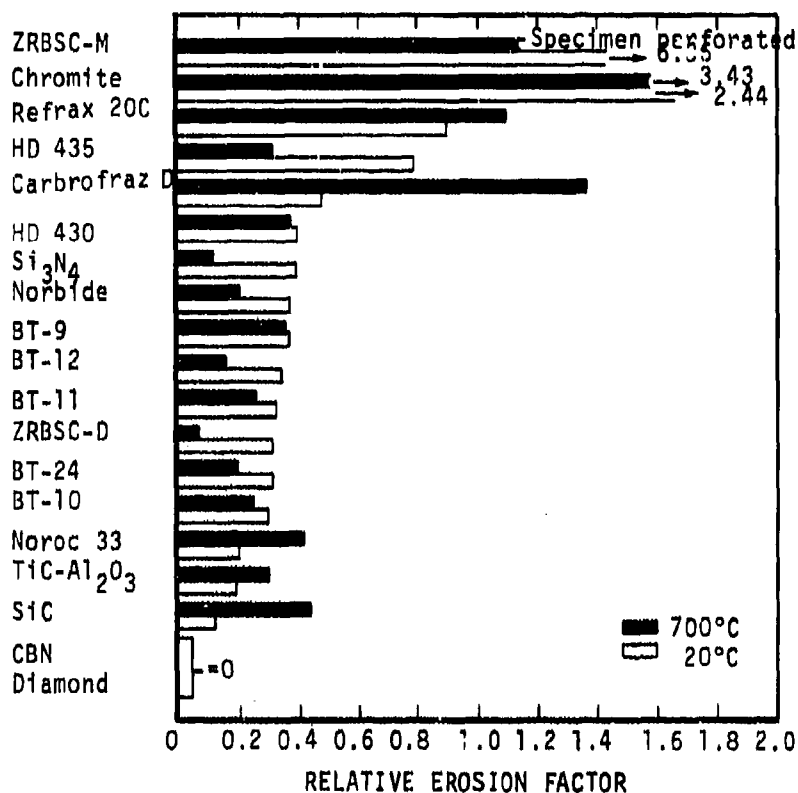


Figure 14. Ceramics (90-Deg Impingement)

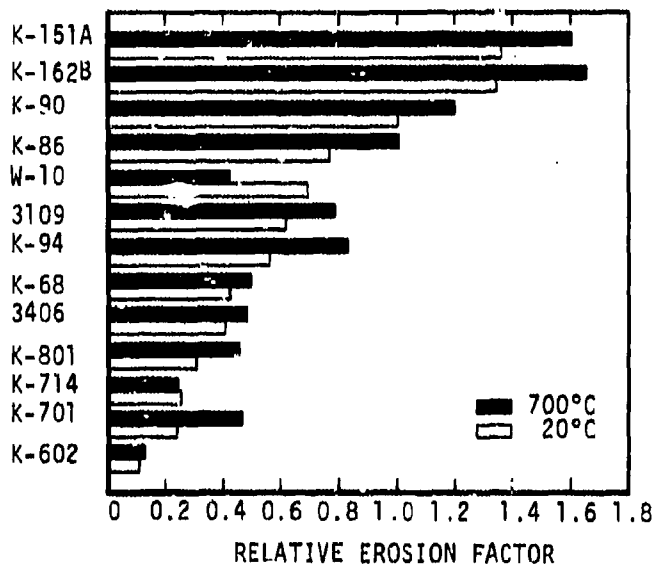


Figure 15. Kennametal Cemented Carbides (90-Deg Impingement)

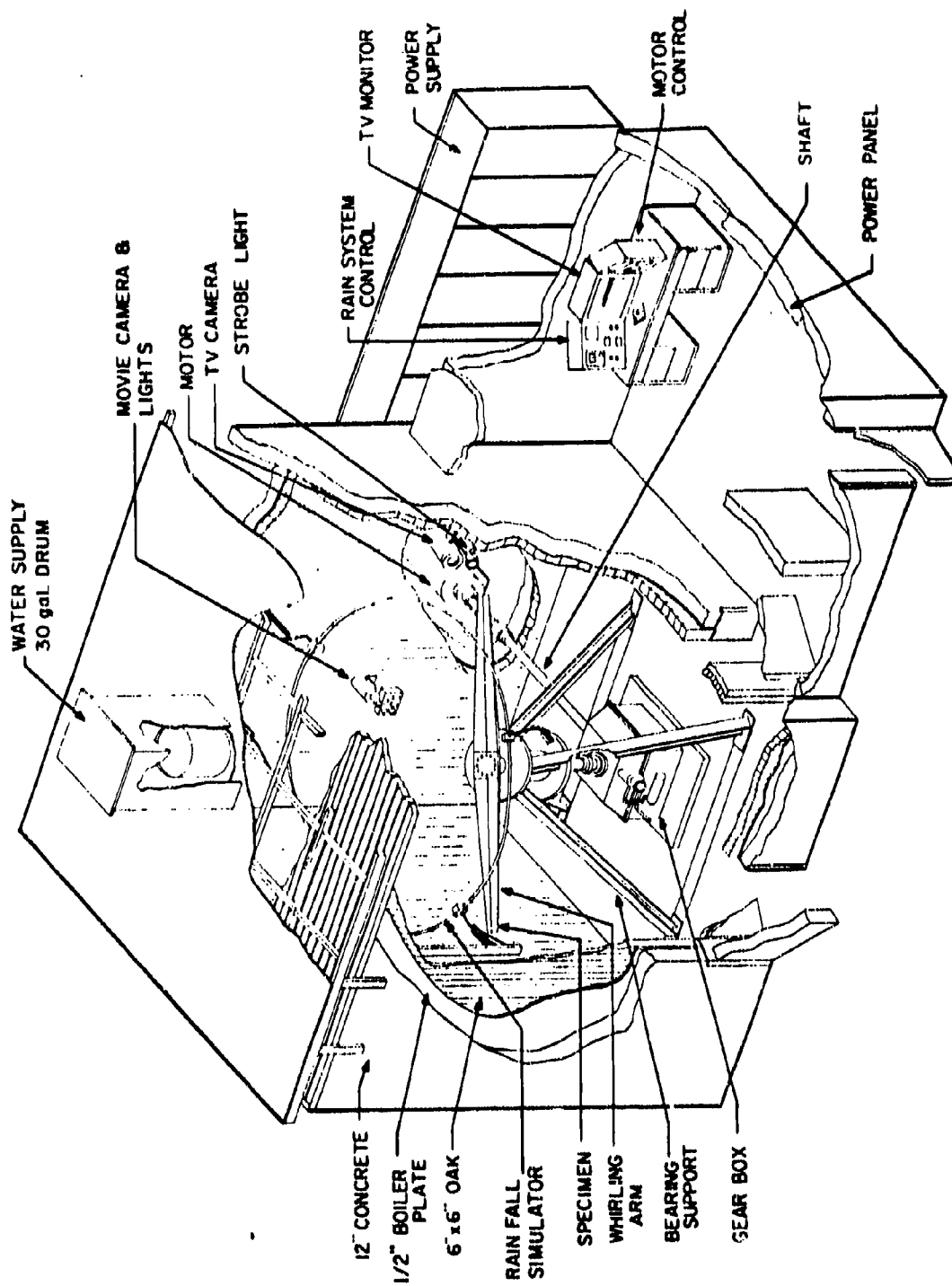


Figure 16. AFML Rotating Arm Apparatus

TABLE 1
 IMPACT CONDITIONS FOR WATER DROPS

Velocity Regime	Eroding Material						
	Rigid	Water	Granular	Brittle	Non-Brittle	Layered	Composite
Free Fall	X	X	X				
Subsonic	X	X		X	X	X	X
Supersonic	X			X	X		X
Hypersonic					X		X

TABLE 2
DESCRIPTION OF DATA AND SYMBOLS USED
IN FIGURES 8 AND 9

Symbol	Material	Velocity (ft/sec)	Diameter of Drop (mm)	Author
△	Parapex	730	1.9	Fyall et al (1957)
▲		1180	1.9	Schmitt et al (1970)
▲		1395	2.0	King (1965)
▽	Alkathane 2	585-730	1.9	Fynll et al (1957)
▼	Q.S.-4 Polyethylene	730	1.9	Fynll et al (1957)
▽	Polyphenylene Oxide	535-3720	1.9	Schmitt et al (1970)
▽	Cast Urethane	730	1.8	Morris et al (1972)
▽	Polypropylene	980-1470	1.2	King (1967)
▶	Teflon	1180	1.9	Schmitt (1970)
○	Aluminum Alloy, D.T.D. 423B	730	1.9	Fyall et al (1957)
●	1100-0 Aluminum	1120	1.8	Morris & Wahl (1970)
◐	1145-H19 Aluminum	1120-2240	1.8	Morris & Wahl (1970)
◑	2024-T6 Aluminum	1120-2240	1.8	Morris & Wahl (1970)
◒	5052-0 Aluminum	1120	1.8	Morris & Wahl (1970)
◓	6061-T6 Aluminum	1120-2240	1.8	Morris & Wahl (1970)

Table 2 (Cont'd)

Symbol	Material	Velocity (ft/sec)	Diameter of Drop (mm)	Author
⊗	7075-T6 Aluminum	1120-2240	1.8	Morrin & Wahl (1970)
		1120		Morris et al (1972)
⊗	Aluminum (Pure)	820-980	1.2	King (1967)
⊗	Aluminum	1650-1420	1.2	Rieger (1965)
⊗	Aluminum Alloys	1340	1.2	Hoff et al (1969)
□	Magnesium Alloy D.T.D. 259	730	1.9	Fyall et al (1957)
◇	Copper Alloy B.S. 1433	585-730	1.9	Fyall et al (1957)
◆	Copper (Electrolytic)	1120	1.8	Morris & Wahl (1970)
■	Nickel	1000	0.866	Engel et al (1971)
▣		1120	1.8	Morris et al (1972)
▤	Cobalt-Chromium Alloys	1020	0.66	Baker et al (1966)
▥	Iron	1000	0.866	Engel et al (1971)
▧	Steels	1020	0.66	Baker et al (1967)
▨		1455	0.64	Herbert (1965)
▩		1120	1.8	Morris et al (1972)

Table 2 (Cont'd)











Symbol	Material	Velocity (ft/sec)	Diameter of Drop (mm)	Author
	Titanium Alloys	1020	0.66	Baker et al (1967)
		1120	1.8	Morris et al (1972)
		1340	1.2	Hoff et al (1965)
	Tantalum	1000	0.866	Engel et al (1971)
	Udimet 700	1000	0.866	Engel et al (1971)
	Magnesia Ceramic	1340	1.2	Hoff (1965)
	Zirconia	1340	1.2	Hoff (1965)
	Alumina Ceramic	1340	1.2	Hoff (1965)
	Spinel	1340	1.2	Hoff (1965)
	Glass	1340	1.2	Hoff (1965)

TABLE 3
 RAIN EROSION EQUATION CONSTANTS: $MDPR = KV^3 \sin^3 \theta$; NOSE TIP MATERIALS

No.	Material	α	Correlation Coefficient, r	K	(MDPR) $\sin^3 \theta$ for $V = 305$ m/s, cm/s	Number of Data Points
Carbon-carbon composites						
T-15	GE orthogonal 3-D (CCAP)	6.652	0.977	7.82×10^{-25}	7.06×10^{-5}	3
T-16	Philo Ford fine weave 3-D (CCAP)	5.243	0.899	1.53×10^{-19}	8.19×10^{-4}	5
T-17	MDAC orthogonal 34-7 3-D (CCAP)	8.242	0.999	1.24×10^{-20}	6.61×10^{-6}	5
T-18	GE polar weave (CCAP)	13.319	0.992	3.53×10^{-20}	3.20×10^{-6}	4
T-19	MDAC 4-4-2 3-D (CERA)	9.777	0.842	2.53×10^{-18}	5.04×10^{-7}	6
T-20	GE 1-3 3-D (CERA)	8.719	0.861	1.44×10^{-12}	2.06×10^{-6}	6
T-21	MDAC 1-1-2 1-D (CHIP)	insufficient data		1
T-22	MDAC 2-2-4 3-D (CHIP)	insufficient data		1
T-23	MDAC 1-D T-50/Tac (CHIP)	insufficient data		1
T-24	AVCO 1-1-5 3-D (CERA)	8.302	0.939	5.75×10^{-21}	4.65×10^{-6}	6
T-25 ^a	GE 1-1-5 3-D (CERA)	6.914	0.883	6.55×10^{-25}	3.62×10^{-5}	5
T-26	GE 1-1-5 3-D (CERA)	insufficient data		2
T-27 ^a	MDAC 1-1-5 4-D (CERA)	9.315	0.791	6.81×10^{-15}	5.99×10^{-7}	5
T-28 ^a	MDAC 1-1-13 3-D (CERA)	8.696	0.921	1.29×10^{-12}	1.59×10^{-6}	5
Graphites						
T-7	ATI-5 graphite	9.491	0.882	5.09×10^{-15}	1.51×10^{-6}	10
T-13	994 improved strain-to-failure graphite	11.103	0.915	3.96×10^{-20}	8.12×10^{-8}	7
T-14	T5-1276 uniform-properties graphite	10.975	0.871	8.53×10^{-14}	7.16×10^{-8}	7

^aMach 4.0 and Mach 5.0, 30-deg cone only; all others are based on at least three runs.

TABLE 4

ROOM TEMPERATURE EROSION TEST RESULTS: 90-DEG IMPINGEMENT, 27- μ m Al_2O_3 PARTICLES, 5-G/MIN PARTICLE FLOW, 170-M/S PARTICLE VELOCITY, 3-MIN TEST DURATION, N_2 ATMOSPHERE

Material	Manufacturing Method	Composition	REF*
99P	ps ^b	99Al ₂ O ₃ (Krohn) ^a	12.49
ZRBSC-M	hp	ZrB ₂ -SiC-graphite(N)	6.36
chromite	ps	(UCAK)	2.44
K151A	ps	19Ni binder (K)	1.37
K162B	ps	28Ni+6Mo binder (K)	1.35
98D	ps	98Al ₂ O ₃ (Krohn)	1.29
T1-6Al-4V	w	...	1.26
Haynes 93	c	17Cr-16Mn-6.3Cn-3C-bal Fe (Stellite)	1.25
Graph-Air	w	1.4C-1.9Mn-1.2Si-1.9Ni-1.5Mo-bal Fe (TRU)	1.19
25Cr Iron	c	26Cr-2Ni-2Mn-0.8Si-3.5C-bal Fe (OGC)	1.19
Stellite 6K	w	30Cr-4.5W-1.5Mo-1.7C-bal Co (Stellite)	1.08
Stellite J	c	31Cr-12.5W-2.4C-bal Co	1.04
K90	ps	28 binder (K)	1.01
Stellite 6B	w	30Cr-4.5W-1.5Mo-1.2C-bal Co (Stellite)	1.00
304 SS	w	17Cr-9Ni-2Mn-18I-bal Fe	1.00
316 SS	w	17Cr-12Ni-2Mn-18I-2.5Mo-bal Fe	0.99
Haynes 188	w	22Cr-14.5W-22Ni-0.15C-bal Co (Stellite)	0.97
Haynes 25	w	20Cr-15W-10Ni-1.5Mn-0.15C-bal Co (Stellite)	0.96
430 SS	w	17Cr-1Mn-18I-0.1C-bal Fe	0.93
HK-40	c	26Cr-20Ni-0.4C-bal Fe	0.93
Inconel 600	w	76Ni-15.5Cr-8Fe (HA)	0.92
RA 330	w	19Cr-35Ni-1.5Mn-1.3Si-bal Fe (HA)	0.91
Refrax 30C	ps	SiC-Si ₃ N ₄ bond (Carbor)	0.91
Incoloy 800H	w	32.5Ni-21Cr-0.07C-46Fe (HA)	0.91
Beta III Ti	w	11.5Mo-6Zr-4.5Sn-bal Ti	0.90
Incoloy 800	w	32.5Ni-46Fe-21Cr (HA)	0.83
HD 435	...	recrystallized SiC (N)	0.80
HA 333	w	25Cr-1.5Mn-1.3Si-3Co-3Mo-3W-18Fe-bal Ni (HA)	0.80
K86	ps	8.8Cu binder (K)	0.78
Inconel 671	w	50Ni-48Cr-0.4Ti (HA)	0.77
Lucalox	...	densified Al ₂ O ₃ (GB)	0.76
mild steel	w	0.15C-bal Fe	0.76
W10	ps	90W-10(Ni, Cu, Fe) (K)	0.70
J109	ps	12.2 binder (K)	0.62
K94	ps	11.5 binder (K)	0.57
Mn	w	...	0.52
Carborax D	ps	SiC-ceramic bond (Carbor)	0.49
W	w	(GB)	0.48
K68	ps	5.8 binder (K)	0.43
J406	ps	7.8 binder (K)	0.42
HD 430	...	recrystallized SiC (N)	0.40
Si ₃ N ₄	hp	(N)	0.40
Norbide	hp	B ₄ C (N)	0.38
BT-9	ps	2MgO-25TiB ₂ -3.5WC-bal Al ₂ O ₃ (OGC)	0.37
BT-12	ps	1.5MgO-49TiB ₂ -3.5WC-bal Al ₂ O ₃ (OGC)	0.35
BT-11	ps	1.7MgO-38TiB ₂ -3.5WC-bal Al ₂ O ₃ (OGC)	0.33
ZRBSC-D	hp	ZrB ₂ -SiC (N)	0.32
VR-54	ps	WC-7Co binder (F)	0.32
BT-24	ps	2MgO-30TiB ₂ -3.5WC-bal Al ₂ O ₃ (OGC)	0.32
K801	ps	6Ni binder (K)	0.32
BT-10	ps	2MgO-30TiB ₂ -3.5WC-bal Al ₂ O ₃ (OGC)	0.30
K714	ps	6Co+1Cr binder (K)	0.26
K701	ps	10.2Co+4Cr binder (K)	0.25
CA 306	ps	WC-6Co binder (Carmet)	0.23
Norox J3	hp	Si ₃ N ₄ -SiC (N)	0.20
TiC-Al ₂ O ₃	ps	(B and W)	0.19
895	ps	WC-6Co binder (Carb)	0.19
SiC	hp	(N)	0.12
K602	ps	<1.5 binder (K)	0.11
SiC	...	(GB)	0.05
CBN	...	(GB)	0
GB diamond	...	(GB)	0

* REF (relative erosion factor) = $\frac{\text{Volume loss material}}{\text{Volume loss Stellite 6B}}$

^b Abbreviations are listed in Table B.

TABLE 5

700°C EROSION TEST RESULTS: 90-DEG IMPINGEMENT, 27- μm Al_2O_3 PARTICLES
5-G/MIN PARTICLE FLOW, 170-M/S PARTICLE VELOCITY, 3-MIN TEST DURATION,
 N_2 ATMOSPHERE

Material	Manu- facturing Method	Composition	REF ^a
ZRBSC-M	hp ^b	ZrB ₂ -SiC-graphite (N) ^b	> 5.00
99P	ps	99Al ₂ O ₃ (Krohn)	> 4.00
chromite	ps	(UCAR)	3.43
K162B	ps	25Ni+6Mo binder (K)	1.67
K151A	ps	19Ni binder (K)	1.62
Stellite J	c	31Cr-12.5W-2.4C-bal Co (Stellite)	1.61
Carbofrax D	ps	SiC-ceramic bond (Carbor)	1.38
895	ps	WC-6Co binder (Carb)	1.32
K90	ps	25 binder (K)	1.21
25Cr Iron	c	25Cr-2Ni-2Mn-0.5Si-3.5C-bal Fe (OGC)	1.16
Refrax 30C	ps	SiC-Si ₃ N ₄ bond (Carbor)	1.15
98D	ps	98Al ₂ O ₃ (Krohn)	1.12
Stellite 6K	w	30Cr-4.5W-1.8Mo-1.7C-bal Co (Stellite)	1.06
K86	ps	8.8Cu binder (K)	1.03
Stellite 6B	w	30Cr-4.5W-1.5Mo-1.2C-bal Co (Stellite)	1.00
Haynes 93	c	17Cr-16Mo-6.3Co-3C-bal Fe (Stellite)	1.00
Haynes 25	w	20Cr-15W-10Ni-1.5Mn-0.15C-bal Co (Stellite)	0.85
K94	ps	11.5 binder (K)	0.84
Haynes 188	w	22Cr-14.5W-22Ni-0.15C-bal Co (Stellite)	0.83
RA 333	w	25Cr-1.5Mn-1.3Si-3Co-3Mo-3W-18Fe-bal Ni (RA)	0.80
3109	ps	12.2 binder (K)	0.80
RA 330	w	19Cr-15Ni-1.5Mn-1.3Si-bal Fe (RA)	0.79
HK-40	c	26Cr-20Ni-0.4C-bal Fe	0.78
304 SS	w	17Cr-9Ni-2Mn-1Si-bal Fe	0.73
Inconel 671	w	50Ni-48Cr-0.4Ti (HA)	0.62
430 SS	w	17Cr-1Mn-1Si-0.1C-bal Fe	0.62
Inconel 600	w	76Ni-15.5Cr-8Fe (HA)	0.61
Lucalox	...	densified Al ₂ O ₃ (GE)	0.57
Beta III Ti	w	11.5Mo-6Zr-4.5Sn-bal Ti	0.57
Incoloy 800	w	32.5Ni-21Cr-46Fe (HA)	0.57
316 SS	w	17Cr-12Ni-2Mn-1Si-2.5Mo-bal Fe	0.56
Ti-6Al-4V	w	...	0.54
Incoloy 800H	w	32.5Ni-21Cr-0.07C-46Fe (HA)	0.54
K68	ps	5.8 binder (K)	0.50
VR-54	ps	WC-7Co binder (F)	0.50
3406	ps	7.8 binder (K)	0.49
K701	ps	10.2Cu+4Cr binder (K)	0.47
K801	ps	6Ni binder (K)	0.46
SiC	hp	(N)	0.44
W-10	ps	90W-10(Ni, Cu, Fe) (K)	0.44
Noroc 33	hp	Si ₃ N ₄ -SiC (N)	0.42
HD 430	...	recrystallized SiC (N)	0.38
CA 306	ps	WC-6Co binder (Carmot)	0.36
BT-9	ps	2MgO-25TiB ₂ -3.5WC-bal Al ₂ O ₃ (OGC)	0.36
HD 435	...	recrystallized SiC (N)	0.32
TiC-Al ₂ O ₃	ps	(B and W)	0.30
BT-11	ps	1.7MgO-38TiB ₂ -3.5WC-bal Al ₂ O ₃ (OGC)	0.26
K714	ps	6Co+1Cr binder (K)	0.25
BT-10	ps	2MgO-30TiB ₂ -3.5WC-bal Al ₂ O ₃ (OGC)	0.25
Norbide	hp	B ₄ C (N)	0.21
BT-24	ps	2MgO-30TiB ₂ -3.5WC-bal Al ₂ O ₃ (OGC)	0.20
W	w	(GE)	0.17
BT-12	ps	1.5MgO-49TiB ₂ -3.5WC-bal Al ₂ O ₃ (OGC)	0.16
K602	ps	< 1.5 binder (K)	0.13
Si ₃ N ₄	hp	(N)	0.12
ZRBSC-D	hp	ZrB ₂ -SiC (N)	0.07
SiC	...	(GE)	0.02
diamond	...	(GE)	0
CBN	...	(GE)	0

^aREF (relative erosion factor) = $\frac{\text{Volume loss material}}{\text{Volume loss Stellite 6B}}$

^bAbbreviations are listed in Table 8.

TABLE 6

ROOM TEMPERATURE EROSION TEST RESULTS ON COATED MATERIALS: 90-DEG IMPINGEMENT, 27- μm Al_2O_3 PARTICLES, 5-G/MIN PARTICLE FLOW, 170-M/S PARTICLE VELOCITY, 3-MIN TEST DURATION, N_2 ATMOSPHERE

Material	Composition and Coating Method	REF ^a
Borofuse Stellite 31 Ni-Cr-B	25Cr-10.5Co-2Fe-7.5W-0.5C-bal Co w/diffused B (MDC) ^b plasma 0.5C-4Si-16Cr-4B-4Fe-2.4Cu-2.4Mo-2.4W-bal Ni (CWS)	1.40 1.32
Borofuse Stellite 6 Cr ₂ O ₃	29Cr-4.5W-1C-bal Co w/diffused B (MDC) plasma Cr ₂ O ₃ -5SiO ₂ -3TiO ₂ (CWS)	1.29 1.23
WC	plasma 3%(WC+8Ni)-11Cr-2.5B-2.5Fe-2.5Si-0.5C-bal Ni (CWS)	1.11
Borofuse Stellite 3 W	31Cr-12.5W-2.4C-bal Co w/diffused B (MDC) pure CVD coating (RMRC)	0.92 0.53
Borofuse MT-104	0.5Ti-0.08Zr-0.03C-bal Mo w/diffused B (MDC)	0.30
Borofuse PM moly	Mo w/diffused B (MDC)	0.25
SIC	CVD SIC on C converted to SIC	0.06
SIC	pure CVD coating	0.05
Borofuse WC	WC w/diffused B (MDC)	0.02
TiB ₂	electrodeposited over Ni (CPMRC)	0
18B-11	TiB ₂ electrodeposited over 310 SS (UT)	0
19A-13	TiB ₂ electrodeposited over 310 SS (UT)	0

^a REF (relative erosion factor) = $\frac{\text{Volume loss material}}{\text{Volume loss Stellite 6B}}$
^b Abbreviations are listed in Table 8.

TABLE 7

700°C EROSION TEST RESULTS ON COATED MATERIALS: 90-DEG IMPINGEMENT, 27- μm Al_2O_3 PARTICLES, 5-G/MIN PARTICLE FLOW, 170-M/S PARTICLE VELOCITY, 3-MIN TEST DURATION, N_2 ATMOSPHERE

Material	Composition and Coating Method	REF ^a
Ni-Cr-B	plasma 0.5C-4Si-16Cr-4B-4Fe-2.4Cu-2.4Mo-2.4W-bal Ni (CWS) ^b	2.79
WC	plasma 3%(WC+8Ni)-11Cr-2.5B-2.5Fe-2.5Si-0.5C-bal Ni (CWS)	2.06
Borofuse Stellite 6	29Cr-4.5W-1C-bal Co w/diffused B (MDC)	1.40
Borofuse Stellite 31	25Cr-10.5Co-2Fe-7.5W-0.5C-bal Co w/diffused B (MDC)	1.37
Borofuse Stellite 3	31Cr-12.5W-2.4C-bal Co w/diffused B (MDC)	0.83
Borofuse WC	WC w/diffused B (MDC)	0.72
Borofuse PM moly	Mo w/diffused B (MDC)	0.28
W	pure CVD coating (RMRC)	0.25
Borofuse MT-104	0.5Ti-0.08Zr-0.03Cr-bal Mo w/diffused B (MDC)	0.19
SIC	pure CVD coating	0
SIC	CVD SIC on C converted to SIC	0
TiB ₂	electrodeposited on Ni (CPMRC)	0
18B-11	TiB ₂ electrodeposited on 310 SS (UT)	0
19A-13	TiB ₂ electrodeposited on 310 SS (UT)	0

^a REF (relative erosion factor) = $\frac{\text{Volume loss material}}{\text{Volume loss Stellite 6B}}$
^b Abbreviations are listed in Table 3.

TABLE 8

ABBREVIATIONS USED IN TABLES 4 AND 7

B and W	Babcock and Wilcox
Carb	Carbonyl Systems Dept., General Electric Corp.
Carbor	Carborundum Co.
Carmot	Carmet Co., Allegheny Ludlum Steel Corp.
e	cast
CPMRC	College Park Metallurgy Research Center
CWS	CWS Corp.
F	Fansteel, Inc.
GE	General Electric Co.
hp	hot pressed
HA	Huntington Alloy Products Div., International Nickel Co.
K	Kennametal, Inc.
Krohn	Krohn Ceramics Corp.
MDC	Materials Development Corp.
N	Norton Co.
OGC	Oregon Graduate Center
ps	pressed and sintered
RMRC	Rolla Metallurgy Research Center
RA	Roller Alloys Corp.
Stellite	Stellite Div., Cabot Corp.
TRB	Timken Roller Bearing Co.
UT	United Technologies Corp.
UCAR	Union Carbide Corp.
w	wrought